AD-A056 251 SRI INTERNATIONAL MENLO PARK CA F/G 9/1
BOLTED LAPPED-JOINT EMP SHIELDS.(U)
JUN 77 A L WHITSON, E F VANCE DNA001-76-C-0386
UNCLASSIFIED DNA-4472F NL

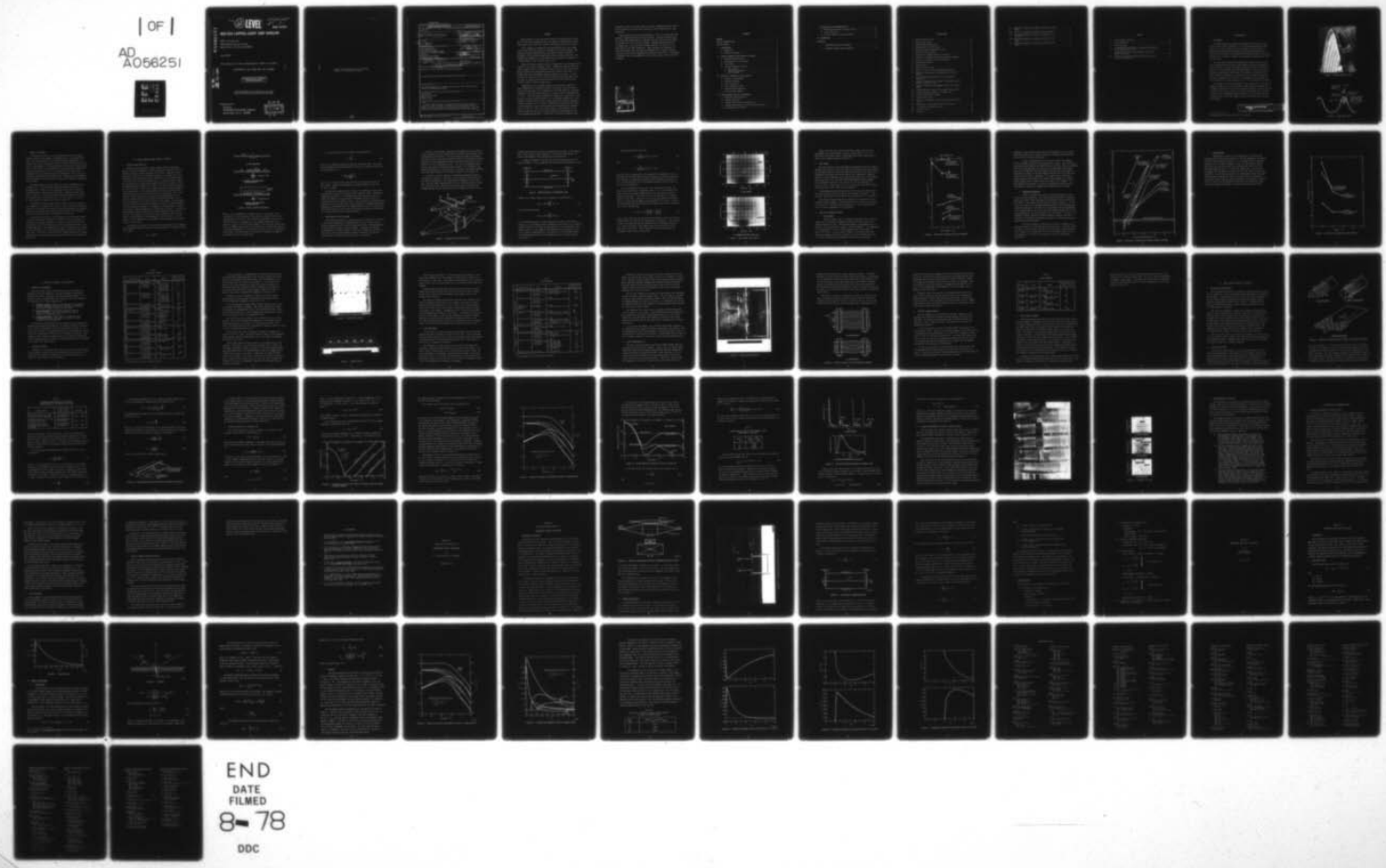

END
DATE FILMED
8-78
DDC

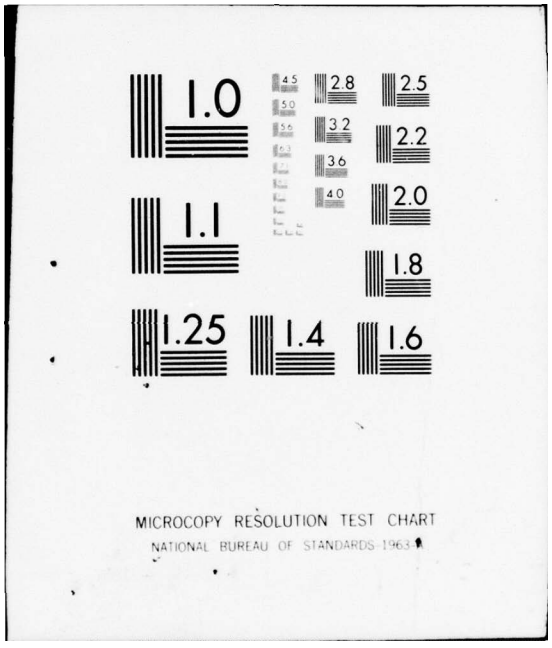
1.0
1.1
1.25
1.4
1.6
1.8
2.0
2.2
2.5
2.8
3.2
3.6
4.0
4.5
5.0
5.6
6.3
MICROCOPY RESOLUTION TEST CHART
NATIONAL BUREAU OF STANDARDS-1963-A

(12) LEVEL II

DNA 4472F

BOLTED LAPPED-JOINT EMP SHIELDS

SRI International
333 Ravenswood Avenue
Menlo Park, California 94025

June 1977

Final Report for Period September 1976—June 1977

CONTRACT No. DNA 001-76-C-0386

THIS WORK SPONSORED BY THE DEFENSE NUCLEAR AGENCY
UNDER RDT&E RMSS CODE B36307T464 O99QAXCA10501 H2590D.

Prepared for
Director
DEFENSE NUCLEAR AGENCY
Washington, D. C. 20305

Destroy this report when it is no longer needed. Do not return to sender.

UNCLASSIFIED

SECURITY CLASSIFICATION OF THIS PAGE *(When Data Entered)*

REPORT DOCUMENTATION PAGE

READ INSTRUCTIONS BEFORE COMPLETING FORM

1. REPORT NUMBER: DNA 4472F
2. GOVT ACCESSION NO.
3. RECIPIENT'S CATALOG NUMBER

4. TITLE *(and Subtitle)*: BOLTED LAPPED-JOINT EMP SHIELDS

5. TYPE OF REPORT & PERIOD COVERED: Final Report for Period September 1976—June 1977

6. PERFORMING ORG. REPORT NUMBER: SRI Project 5785

7. AUTHOR(s): A. L. Whitson, E. F. Vance

8. CONTRACT OR GRANT NUMBER(s): DNA 001-76-C-0386

9. PERFORMING ORGANIZATION NAME AND ADDRESS: SRI International, 333 Ravenswood Avenue, Menlo Park, California 94025

10. PROGRAM ELEMENT, PROJECT, TASK AREA & WORK UNIT NUMBERS: NWED Subtask Ø99QAXCA105-01

11. CONTROLLING OFFICE NAME AND ADDRESS: Director, Defense Nuclear Agency, Washington, D.C. 20305

12. REPORT DATE: June 1977

13. NUMBER OF PAGES: 84

14. MONITORING AGENCY NAME & ADDRESS *(if different from Controlling Office)*: DNA, SBIE

15. SECURITY CLASS *(of this report)*: UNCLASSIFIED

15a. DECLASSIFICATION/DOWNGRADING SCHEDULE

19. 4472F, AD-E300 255

16. DISTRIBUTION STATEMENT *(of this Report)*

Approved for public release; distribution unlimited.

17. DISTRIBUTION STATEMENT *(of the abstract entered in Block 20, if different from Report)*

18. SUPPLEMENTARY NOTES

This work sponsored by the Defense Nuclear Agency under RDT&E RMSS Code B36307T464 O99QAXCA10501 H2590D.

19. KEY WORDS *(Continue on reverse side if necessary and identify by block number)*

EMP Shielding
Lapped-Joint Leakage
Bolted Joints
Riveted Joints

20. ABSTRACT *(Continue on reverse side if necessary and identify by block number)*

Bolted, nonwelded joints in shields leak electromagnetic energy of frequencies above a few MHz. Overlapping joints have been measured to define joint characteristics that can be used for EMP shields. Also some nonideal joints were measured to determine joint quality requirements.

DD FORM 1 JAN 73 1473 EDITION OF 1 NOV 65 IS OBSOLETE

UNCLASSIFIED

SECURITY CLASSIFICATION OF THIS PAGE *(When Data Entered)*

410 281

JOB

SUMMARY

EMP shields are often continuous welded (or soldered) metal liners for the facility or equipment room. The effect on shielding by joining liner panels with bolted (or rivited) overlapping joints is not known.

Joint leakage, as measured by the polarizability per unit length of the joint, has been found to be dependent on fastener spacing. The leakage increased approximately as the cube of fastener spacing in accordance with theoretical predictions based on long, thin slits. The leakage also depended to a small degree on bolt torque and somewhat to a larger degree on the overlap at the joint.

Among the quality control factors, cleanliness of the mating surfaces appears to be the most important factor. Leakage through the joint increases significantly if contaminants such as rust or scale prevent the mating surfaces from making good electrical contact at the joint. It appears that such contaminants enhance leakage in two ways: (1) they increase the effective size of the crack between the joined parts, and (2) they can increase the effective fastener spacing if they prevent fastener contact with the joined parts.

Comparisons of the voltages incuded on an internal conductor by joint leakage and by diffusion through a jointless, 1-mm thick steel shield indicated that at all frequencies in the EMP spectrum, joint EMP leakage is no greater than diffusion for typical joints (polarizability $m \approx 10^{-6}$). When the induced voltages are compared as a function of time, however, the peak voltage induced on a long internal conductor by joint leakage is greater than the peak voltage induced by diffusion through a jointless shield (0.5 V vs 0.3 mV), although the duration of the joint-related transient is much shorter than the diffusion-related transient (10 ns vs 200 μs). Thus, the coupled energy is much greater for the diffusion-induced pulse, but the peak voltage is much greater for the joint-leakage-induced pulse. In addition, the diffusion-induced pulse

is additive over a long wire within a facility, whereas the joint related pulse, because of its very short duration, is not cumulative over long conductors.

Good overlap joints with polarizability of 10^{-7} can be made for EMP shields if panels have metal-to-metal contact. Aluminum and galvanized steel have been demonstrated to make good contact with contact pressures as provided by 3 to 4 m-kg bolt torques. Fastener spacings should be no larger than 7.5 cm, and joint overlap should be at least 10 cm for good joints at all EMP frequencies. Rope caulking (3 mm diameter) in the joint between the joint edge and fasteners can be used to provide a moisture seal without degrading the shielding of the joint. Preferrably a waterproof seal is recommended over the outer surface of the joint and fasteners.

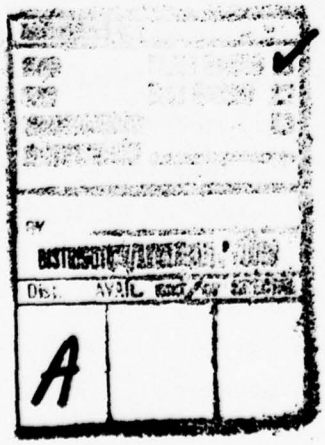

CONTENTS

ILLUSTRATIONS

TABLES

I INTRODUCTION

A. BACKGROUND

The construction cost savings associated with using the aircraft shelter liner[1]* shown in Figure 1 as a self-supporting structure that serves as a concrete form and at the same time as an EMP shield is recognized as an attractive solution to EMP hardening requirements. However, the usefulness of the approach has been questioned on the basis that there are no data to indicate the shielding effectiveness of such a steel liner.

The uncertainty about EMP shielding effectiveness arises because the corrugated panels that make up the shelter are bolted together, as shown in Figure 2, rather than welded (welding has been the standard practice for constructing continuous EMP shields). Any question about shielding effectiveness that arises from leakage and possible arcing along the panel attachments or joints could be eliminated by welding the panels together after erection. Unfortunately, this approach not only increases the costs significantly but also compromises the concept.

The purpose of the work described in this report was to evaluate the leakage through joints in sheet metal so that questions regarding the shielding effectiveness of various fastening techniques could be resolved. To achieve this goal, a series of controlled experiments was conducted to measure the fundamental leakage parameters on test panels that had riveted, bolted, and welded joints with various natural and simulated contaminants.

*References are listed at the end of the report.

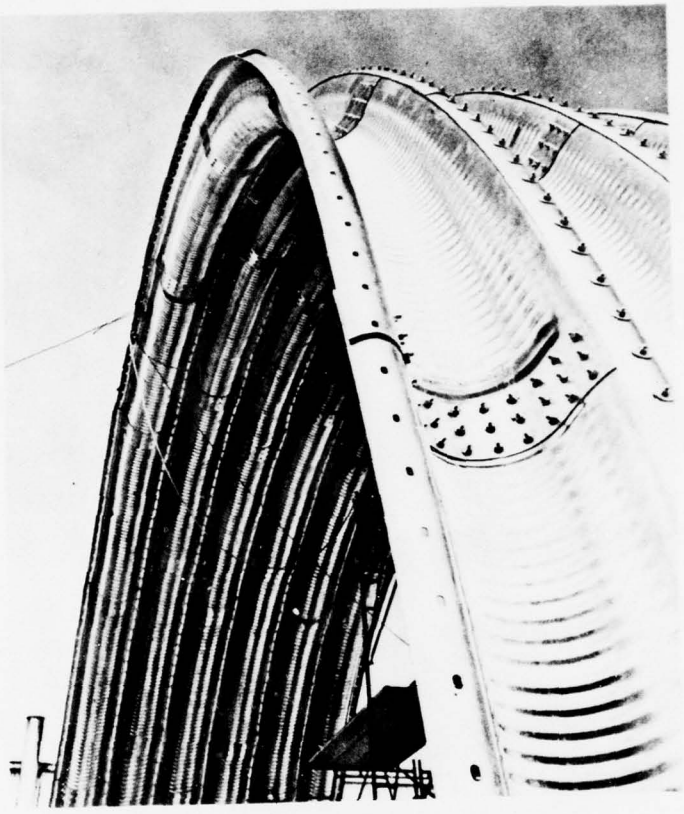

FIGURE 1 AIRCRAFT SHELTER LINER

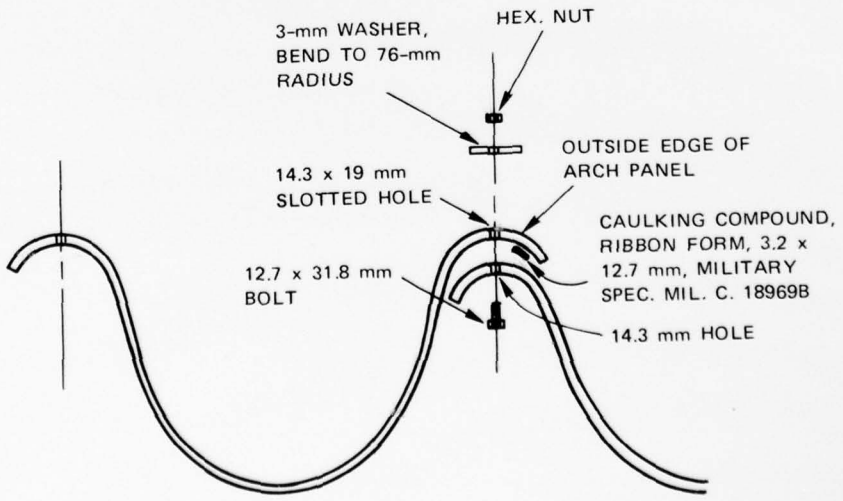

FIGURE 2 LINER PANEL JOINTS

B. METHOD OF APPROACH

As described in Section II, the fundamental measure of leakage through a joint is the magnetic polarizability per unit length of the joint. The polarizability is the effective dipole strength of the leakage field on the "protected" side of the shield produced by one unit (e.g., 1 ampere/meter) of excitation field at the outside ("unprotected" side) of the shield. The polarizability thus relates the leakage field to the excitation field, and it is a property of the shield that is independent of the excitation source and independent of the circuits or structures responding to the leakage field. Because the polarizability can be measured, it was chosen as the quantitative measure of shielding effectiveness.

The polarizability per unit length of joints was measured in the laboratory for: riveted, bolted, and sheet-metal-screw joints in aluminum sheet; bolted joints in galvanized steel sheet; and bolted and welded joints in hot-rolled steel sheet. Parametric studies were made to evaluate: the effects of fastener spacing; amount of overlap at the joint; and for bolts, the effect of bolt torque. The results of these parametric studies are given in Section II.

In addition, several quality control, aging, and "fix" properties were examined. For example, the effects of rust, scale, and insulating material in the joints were examined, and the effectiveness of conductive epoxy resins and copper foil tape as shield "patches" were evaluated. These tests and the results are discussed in Section III.

To evaluate the effect of joint leakage on the environment inside a facility constructed of panels with joints of the types tested, the voltage per unit length induced on a conductor inside a facility was calculated from the polarizability and the two-exponential model of the incident EMP field. For comparison, the induced voltage per unit length was also calculated for a continuous (no joints) shield of 1-mm thick, mild steel. The results of these induced voltages estimates and leakage measurements on full-scale aircraft liner panel joints are presented in Section IV.

II LEAKAGE THROUGH LAPPED JOINTS IN SHIELDS

A. LEAKAGE CHARACTERISTICS

Leakage of electromagnetic fields through joints in sheetmetal shields is caused by imperfect contact between the joined parts and by apertures (cracks or other openings) at the joint. Imperfect contact produces an increase in the surface resistance at the joint and a corresponding $j(t)R_j$ voltage across the joint [$j(t)$ is the current density in A/m and R_j is the joint resistance in mΩ]. Apertures permit some of the external fields to penetrate through the shield to interior wiring or equipment where voltages of the form M dj/dt and currents of the form C dv/dt are induced. The M dj/dt voltages are associated with magnetic field penetrating to the interior region, and they are excited by the current density j(t) on the outside surface of the shield. The C dv/dt currents are associated with the electric field penetrating to the interior region, and they are excited by the shield potential v(t) or the charge density on the outside surface of the shield. For overlapped joints with 100 percent optical coverage, the electric field penetration is often negligible compared to the magnetic field penetration. These three shield leakage mechanisms are illustrated in Figure 3. In addition, some magnetic field penetrates (or diffuses through) the sheet metal. However, this leakage is very small at high frequencies where the skin depth is small compared to the thickness of the sheet metal. In this report, we will concentrate on the magnetic field leakage through lapped joints in sheet metal.

According to the theory of electrically small apertures, the magnetic field fringing through an aperture can be represented by a magnetic dipole of strength

$$P_m = \mu_o H_o(t) m \quad , \tag{1}$$

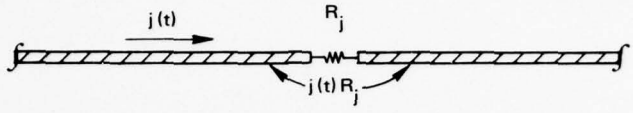

(a) JOINT RESISTANCE

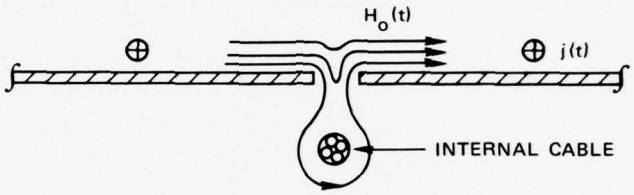

(b) MAGNETIC FIELD PENETRATION THROUGH APERTURE

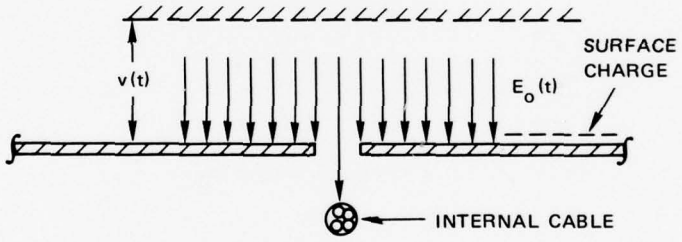

(c) ELECTRIC FIELD PENETRATION THROUGH APERTURE

FIGURE 3 SHIELD LEAKAGE MECHANISMS

where μ_o is the permeability of space, $H_o(t)$ is the magnetic field intensity that would be present if the hole were absent, and m is the polarizability of the hole. The polarization depends on the size and shape of the hole; m contains all of the leakage properties of the aperture; $\mu_o H_o(t)$ is the "external" magnetic field exciting the aperture. Thus, the leakage properties of holes and joints in shield materials can be compared independent of the structure (such as cables) or measurement method (loop size and distance from shield) by comparing the magnetic polarizabilities of these apertures.

For circular apertures, the magnetic polarizability is[2]

$$m = \frac{4r_o^3}{3} \quad . \tag{2}$$

That is, the leakage increases as the cube of the hole size. For long, thin elliptical slits with the magnetic field $H_o(t)$ parallel to the slit, the polarizability is[2]

$$m = \frac{\pi}{24} \frac{\ell^3}{\ln\left(\frac{4\ell}{W}\right) - 1} \quad , \tag{3}$$

where ℓ is the length (major axis) and W is the width (minor axis) of the ellipse. Again the polarizability increases roughly as the cube of the slit length.

The apertures between rivets or bolts in a sheetmetal joint may be visualized as a series of long, thin slits along the joint. Because the leakage through each slit is combined with that from every other slit inside the shield, we can represent the leakage through a joint by a polarization per unit length of joint. Also, because the openings between lapped joints have a depth equal to the overlap, the leakage through these openings is much smaller than the leakage through a slit in a thin sheet. The formulas above for the circular and elliptical apertures were derived for an infinitesimally thin conducting sheet.

B. MEASUREMENT OF JOINT LEAKAGE

Since the polarizability of the apertures in a shield is the measure of the shield leakage and is independent of the size or shape of the shielded enclosure formed from the shielding material, the polarizability is the preferred measure of shield leakage. To measure the magnetic polarizability, a uniform magnetic field must be applied to one side of the shield, and the induced magnetic dipole strength of the excited aperture must be measured on the other side of the shield.

Because of reflections, resonances, and leakage around the shield, direct measurement of the induced dipole strength in the presence of the exciting field is difficult. One can, however, provide the necessary isolation between the excitation and the detection instruments by enclosing both in closed transmission lines with the test specimen in a wall shared by the two transmission lines.[3] The use of rectangular transmission lines permits uniform excitation fields to be developed, and matched terminations on the detection, or sensing, line prevent standing waves that make analysis of the results difficult (see Appendix A).

A sketch of a tester using two rectangular transmission lines is illustrated in Figure 4. The lower line is driven by an RF source at one end and terminated in its characteristic impedance at the other end. The test panel containing the joint to be measured forms a common wall between the lower (driving) line and the upper (sensing) line. Leakage through the test panel excites the sensing line and develops a

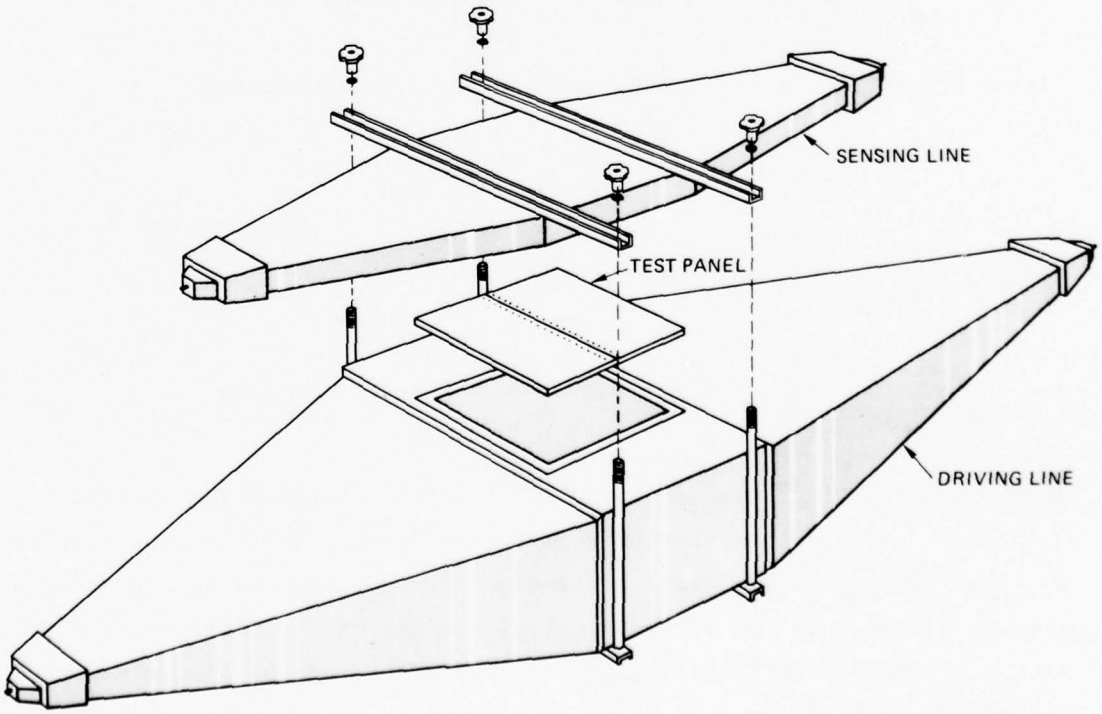

FIGURE 4 EXPLODED VIEW OF SKIN TESTER

voltage across each of the match terminations at the ends of the sensing line. Small loop and dipole antennas in the driving line measure the electric and magnetic field strength in the driving line.

A schematic diagram of the aperture coupled transmission lines is shown in Figure 5. For an aperture with both electric and magnetic field

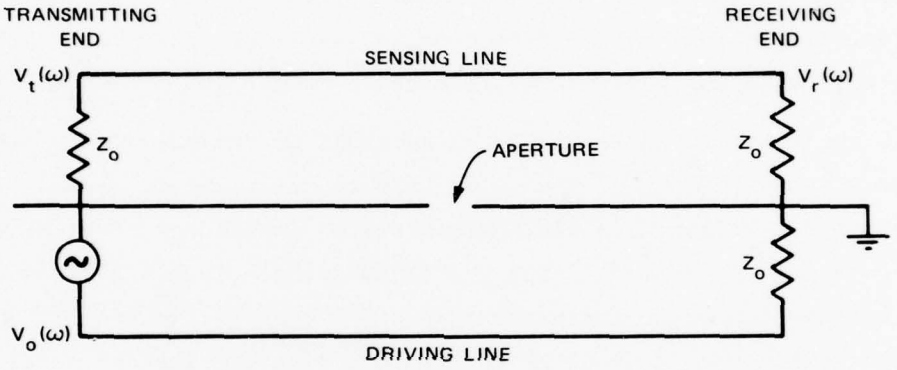

FIGURE 5 APERTURE-COUPLED TRANSMISSION LINES

leakage, the voltage induced in the sensing line terminations is

$$V_r(\omega) = j\omega K \frac{V_o(\omega)}{2Z_o} (m - p) \tag{4}$$

at the receiving end and

$$V_t(\omega) = j\omega K \frac{V_o(\omega)}{2Z_o} (m + p) \tag{5}$$

at the transmitting end. In these expressions, $V_o(\omega)$ is the driving voltage, Z_o is the characteristic impedance of the lines, K is a coupling constant related to the cross section geometry of the rectangular transmission lines, m is the magnetic polarizability of the aperture, and p is the electric polarizability of the aperture [p is the dipole moment of the penetrating electric field normalized to the exciting electric flux $\epsilon_o E_o(\omega)$].

The polarizabilities are thus,

$$m = \frac{Z_o}{j\omega V_o(\omega)K}\left[V_t(\omega) + V_r(\omega)\right] \tag{6}$$

and

$$p = \frac{Z_o}{j\omega V_o(\omega)K}\left[V_t(\omega) - V_r(\omega)\right] \quad . \tag{7}$$

$V_t(\omega)$ and $V_r(\omega)$ are measured at the sensing line terminations, $V_o(\omega)$ is obtained from the small loop or dipole antenna in the driving line, and K is obtained by calibrating the tester with calculable apertures such as a circular aperture, or for distributed apertures such as joints, a row of circular apertures.

For the overlapped joints used in the tests described here, the electric polarizability is negligible and $m + p \approx m$. In addition, for these joints, the leakage (polarizability) is much greater when the magnetic field $H_o(\omega)$ is parallel to the joint than when it is perpendicular to the joint. Thus, all but a few of the polarization measurements were made with the magnetic field parallel to the joint. Using K for distributed apertures and using the voltage on the loop field sensor $V_\ell(\omega)$ in the driving line,

$$m = -7.66j \times 10^{-3}\left[\frac{V_t(\omega)}{V_\ell(\omega)} + \frac{V_r(\omega)}{V_\ell(\omega)}\right] \quad . \tag{8}$$

$V_t(\omega)$, $V_r(\omega)$, and $V_\ell(\omega)$ all increase with frequency so that the measured voltage ratios are constant and independent of frequency. For the panels tested, the voltage ratios were measured from 1 to 100 MHz using swept CW. Figure 6(a) shows a data sample taken at the receive end of the sense line, $V_r(\omega)/V_\ell(\omega)$. Three readings at 20, 50, and 80 MHz were averaged to obtain each voltage ratio.

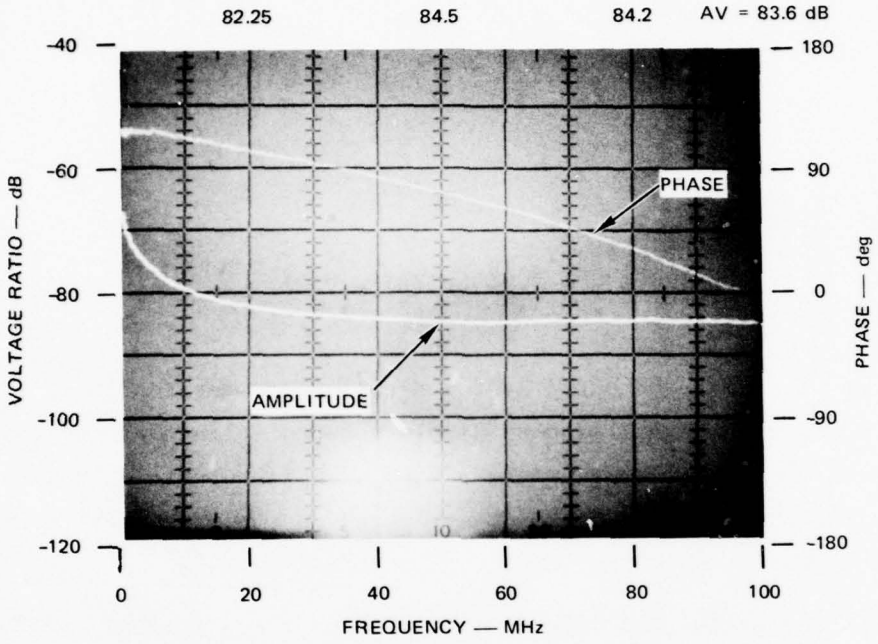

(a) DATA SAMPLE

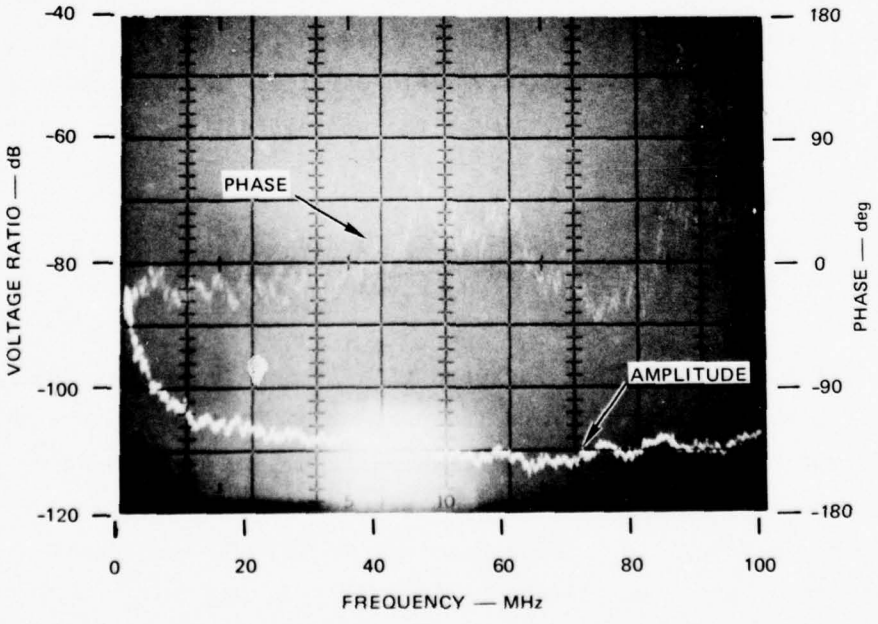

(b) MINIMUM DETECTABLE SIGNAL (noise)

FIGURE 6 SKIN TESTER DATA DISPLAY

Figure 6(b) shows the minimum detectable voltage ratio for the overlapping joint measurements. Using a voltage ratio of 0.7×10^{-5} (103 dB) as the minimum useable measurement, the minimum polarizability that can be reliably measured is about 10^{-7}.

C. TEST PANELS

The test panels for the polarizability measurements are 50-cm square samples with the joint across the middle of the panel as shown in Figure 4. The shielding materials tested included aluminum sheet with bolted joints, galvanized steel sheet with bolted joints, some commercially prepared samples of riveted aluminum, and a shielded-room structure. Most measurements were made on 3.17-mm thick 6061-T6-QQ-A-250/11 aluminum panels. Joint overlaps tested were 5, 10, and 15 cm with bolt spacings of 5, 11.5, and 23 cm. Bolts were 12.7-mm (1/2 inch) steel, with flat washers. Bolt holes were 14.3 cm (9/16 inch in diameter).

The galvanized steel test panels were 3-mm thick cold rolled steel with bolts and bolt holes the same as the aluminum test panels. Joint overlaps tested were 5 and 10 cm with bolt spacings of 7.5, 9, and 18 cm.

The riveted aluminum panels were standard van construction with a Z-shaped stiffner channel. Joint overlap was 5 cm, with rivet spacings of 5 and 13 cm. One panel was tested that had 7.5-cm overlap and two rows of rivets (staggered) on 5-cm spacings.

D. LEAKAGE MEASUREMENT RESULTS

1. Bolt Torque

Tests of bolted joints in aluminum, galvanized steel, and hot-rolled steel were made to evaluate the effect of bolt torque on the leakage through the joint. The measured magnetic polarizabilities per meter of joint are plotted in Figure 7 for these samples. For comparison, the polarization of a row of 12.5-mm diameter holes 25 mm apart is 13.4×10^{-6} m^3/m. As can be seen in Figure 7, the bolted joints all have less leakage than the row of holes, but the hot-rolled steel with 7.5-cm bolt spacing was only slightly better than the open holes.

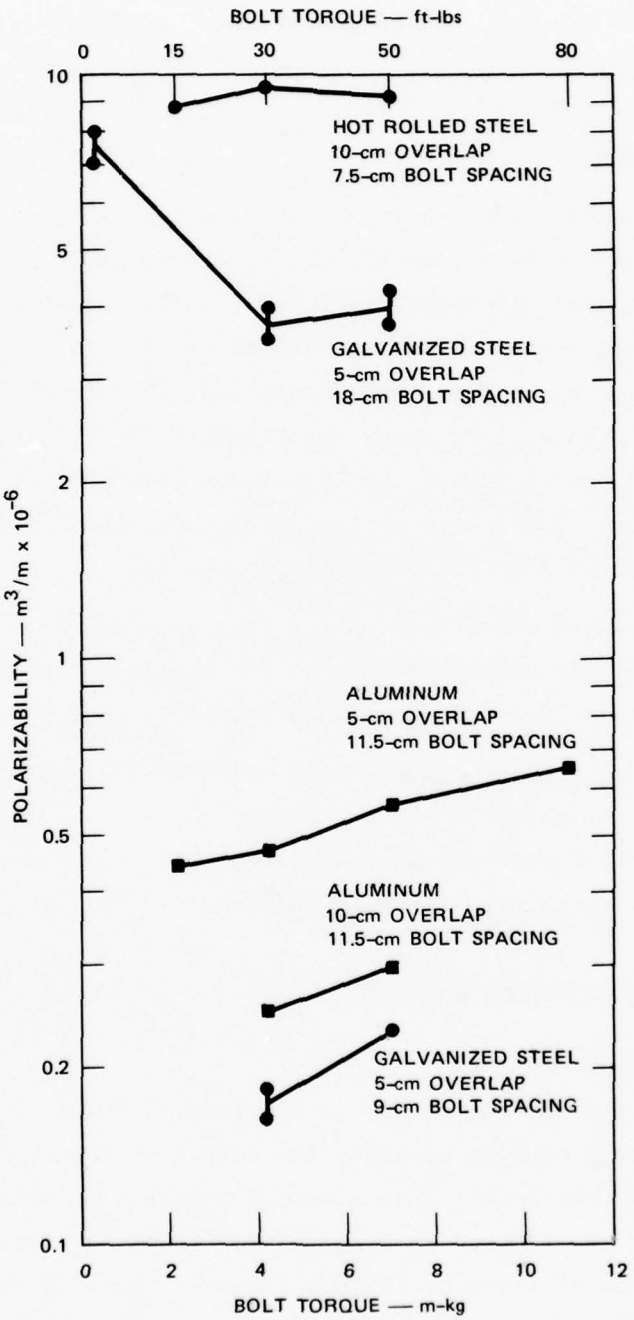

FIGURE 7 VARIATION IN LEAKAGE WITH BOLT TORQUING

Subsequent tests indicated that this poor performance of the hot-rolled steel was caused by poor contact between the overlapped pieces because of the scale on the hot-rolled sheet.

A very interesting result of the test is that the leakage tends to increase slightly with increasing bolt torque. This apparently is caused by the bowing of the metal sheets as the bolt torque is increased. Tests with hand-tight bolts (0 torque) on the galvanized steel sample with 10-cm overlap and 18-cm bolt spacing indicate that the leakage is significantly larger for the hand-tight bolts than for 4 m-kg (30 ft-lb) or more of bolt torque. Therefore, it is apparent that some torque greater than zero is required for minimum joint leakage, but excessive torque (greater than 4 m-kg) causes an increase in the leakage. It is also apparent from Figure 7 that the bolt spacing and overlap produce much greater variations in leakage than variations in bolt torque.

2. Spacing of Fasteners

Tests to determine the effect of spacing between bolts and rivets were also conducted. Both riveted and bolted panels of aluminum sheet were tested, and bolted panels of galvanized and hot-rolled steel were tested. The results of these tests are shown in Figure 8. As can be seen in Figure 8, the leakage increases rapidly with increasing spacing between fasteners. This behavior is consistent with the dependence of the polarization on the cube of the slit length indicated earlier and is demonstrated by the curve labeled $0.01\ \ell^3$ in Figure 8. There is considerable variation among the different samples, however, and this is presumed to be caused by differences in quality of contact and amount of bowing out between fasteners.

One test was made to determine the effect of a double row of fasteners using the riveted aluminum van construction. This data, shown in Figure 8, indicate that a second row of rivets give some improvement over a single row. Overlap was 7.5 cm for the double row and 5 cm for the single row of rivets, which accounts for some of the measured improvement.

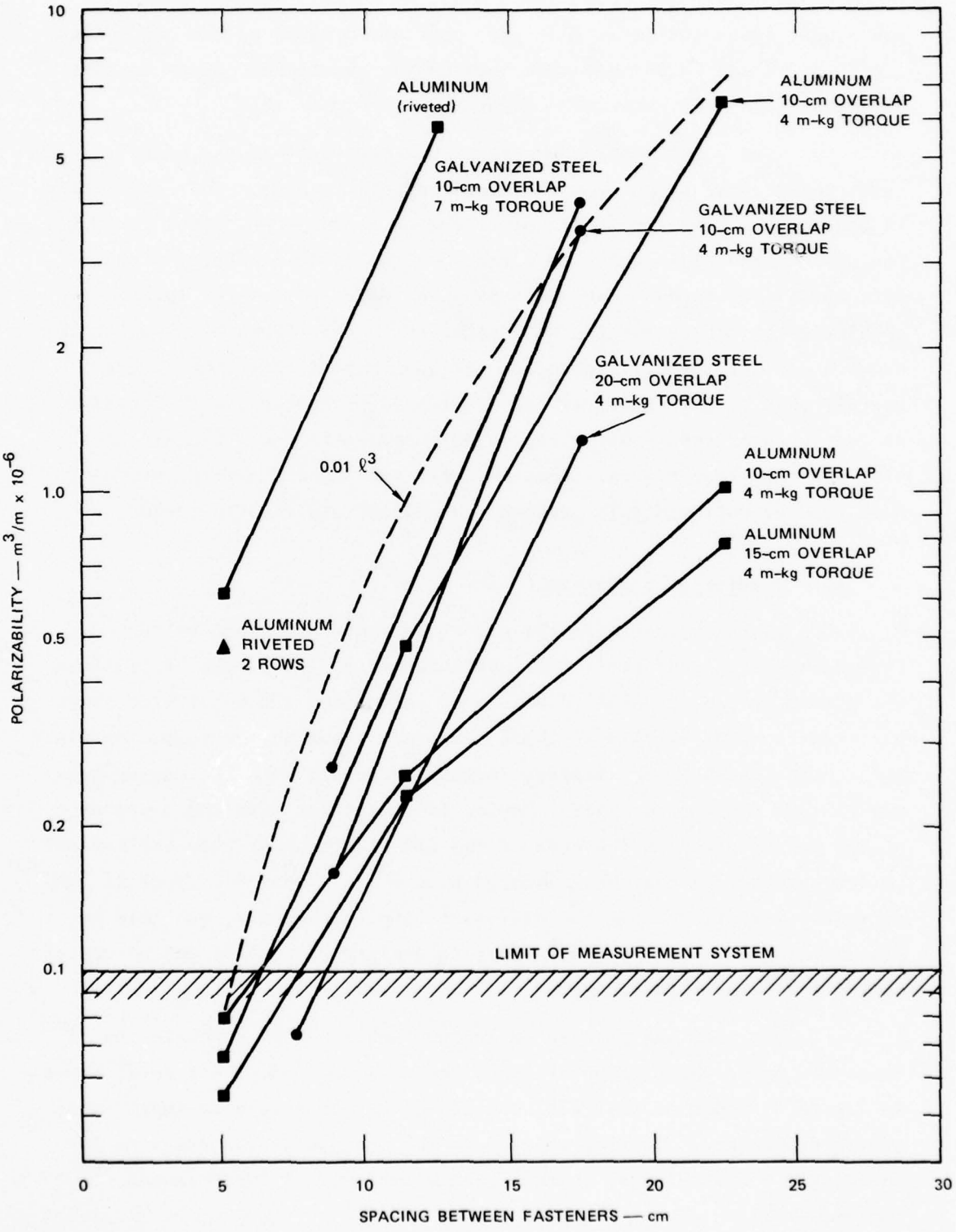

FIGURE 8 VARIATION IN LEAKAGE WITH SPACING BETWEEN FASTENERS

3. Joint Overlap

Variations in overlap of the lapped joints in aluminum and galvanized steel panels were tested for a few bolt spacings. The results of these tests are shown in Figure 9. It is apparent that the leakage decreases as the overlap increases, but for the two aluminum samples, which were the only ones tested with overlap greater than 10 cm, the decrease between 10 and 15 cm is not very significant. This decrease in leakage may be because of the depth of the crack that the fields must penetrate. At very high frequencies, the capacitance between the lapped pieces probably permits the current to cross the gap as displacement current with little magnetic pulse penetrating to the interior. Measurements for bolts on 5-cm spacings were all below the measurement sensitivity (see Figure 8) and show no consistent variation with overlap.

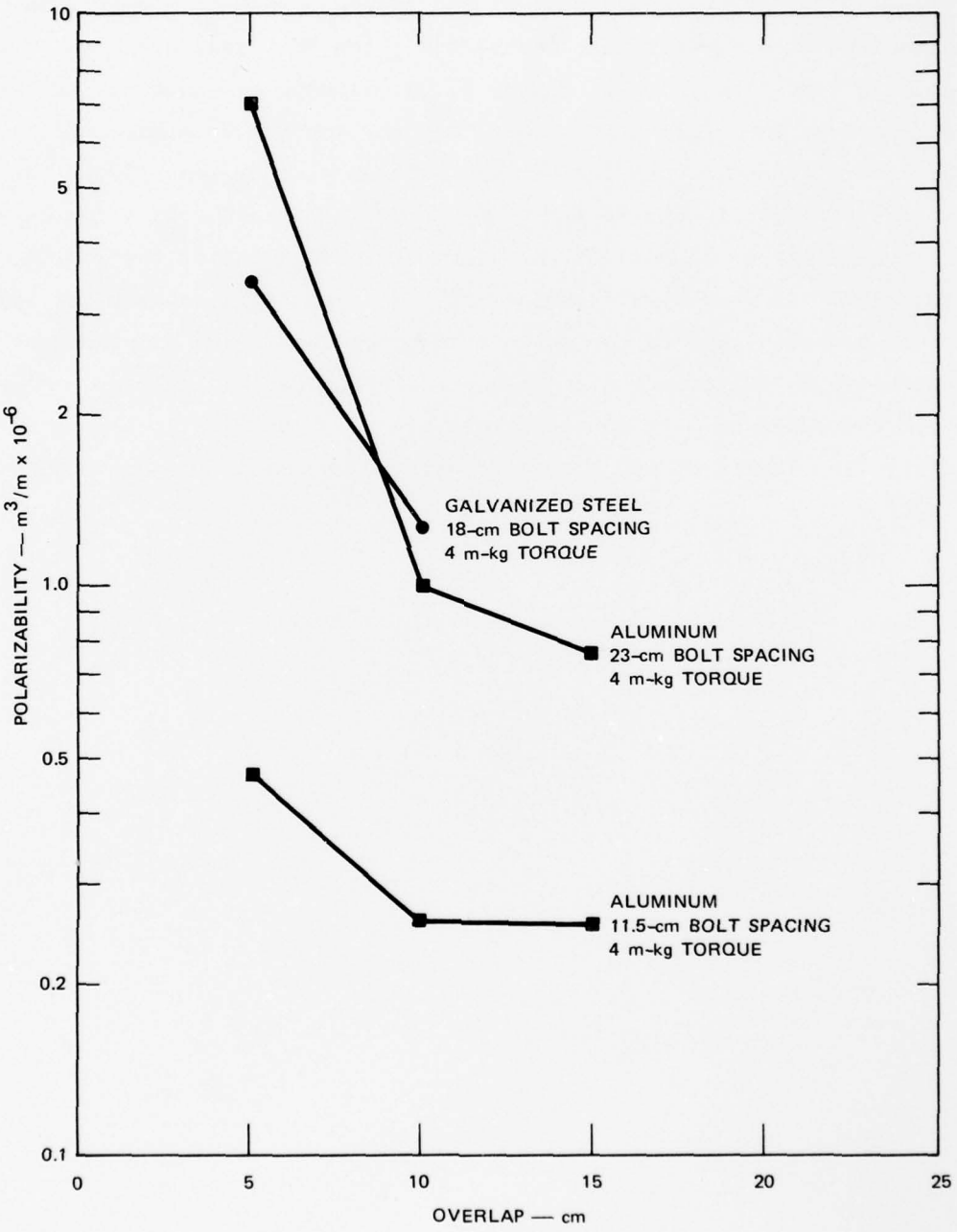

FIGURE 9 VARIATION IN LEAKAGE WITH JOINT OVERLAP

III EFFECTS OF CHANGES IN JOINT QUALITY

A. PURPOSE OF MEASUREMENTS

Many variations in joint quality were tested to determine the sensitivity of joint leakage to test panel preparation procedures, assembly procedures, treatments, and shield patching schemes. The effects of these variations have been separated into three categories for reporting here. These categories are:

(1) Assembly Problems, which include painted or contaminated surfaces, distorted plates, and variations in fasteners that might accompany assembly of the joints.

(2) Joint Treatments, which include conductive fillers, metal foil gaskets, and tack welding that might be proposed to improve the joint.

(3) Patching Materials, which consist of conductive epoxy and copper foil tape that might be proposed to patch a leaky joint after assembly.

The effects of these variations and treatments were evaluated by measuring the magnetic polarizability of specially prepared test panels in the coaxial transmission line tester described in Section II. In each case, a "normal" or pretreatment panel was also measured to provide a basis for evaluating the effects of the treatment or variation. The results of these tests are presented for each of the three categories in the following sections in terms of the polarizability per unit length of the normal and variant joints.

B. ASSEMBLY PROBLEMS

Variations in joints that might occur as a result of material handling, assembly, and aging have been subdivided into four groups. The shielding effectiveness, as measured by the polarizability per unit length, for each sample is given in Table 1.

Table 1

JOINT ASSEMBLY PROBLEMS

	Panel Material	Joint	Problem	Polarizability ($m^3/m \times 10^{-6}$)
Simulated Surface Contaminants	Galvanized steel	10-cm overlap 18-cm bolt spacing (3 bolts) 4 m-kg torque	1. None 2. One 7.5-cm wide plastic strip 3. Two 7.5-cm wide plastic strips 4. 0.13-mm plastic spacer in joint	1.3 3.0 4.5 35
	Galvanized steel	5-cm overlap 9-cm bolt spacing (5 bolts) 4 m-kg torque	1. None 2. One 2.5-cm wide plastic strip 3. Two 2.5-cm wide plastic strips 4. Four 2.5-cm wide plastic strips	0.16* 0.43 0.56 0.53
	Galvanized steel	10-cm overlap 7.5-cm bolt spacing (6 bolts)	1. None 2. Five 2.5-cm wide plastic strips	0.08* 0.26
Surface Contamination	Aluminum riveted panels	5-cm overlap 5-cm spacing	1. None 2. Painted surface	0.63 3.1
	Hot rolled steel	10-cm overlap 7.5-cm bolt spacing (6 bolts) 4 m-kg torque	1. None (galvanized steel) 2. Surface scale 3. Surface scale removed	0.08* 9.9 1.3
	Cold rolled steel	10-cm overlap 7.5-cm bolt spacing (6 bolts) 4 m-kg torque	1. None (galvanized steel) 2. Rusty joint	0.08* 190
Panel Distortion	Galvanized steel	5-cm overlap 18-cm bolt spacing (3 bolts) 4 m-kg torque	1. None 2. Warped panels	4.0 4.1
	Galvanized steel	10-cm overlap 7.5-cm bolt spacing (6 bolts) 4 m-kg torque	1. None 2. Warped panels 3. Bent up edges	0.08* 0.1* 0.29
Joint Hardware	Hot rolled steel	10-cm overlap 7.5-cm bolt spacing (6 bolts) 4 m-kg torque	1. None (flat washers) 2. Lock washers	2.2 2.5
	Galvanized steel	10-cm overlap 9-cm bolt spacing (5 bolts) 4 m-kg torque	1. None 2. Rubber washers under bolts and nuts	0.16* 0.21
	Galvanized steel	10-cm overlap 7.5-cm bolt spacing (6 bolts) 4 m-kg torque	1. None 2. 3-mm rope caulking in joint	0.16* 0.26

*This measurement is near the measurement threshold.

In the first group, a contaminated or corroded surface condition was simulated by installing plastic film (0.13 mm) between the mating surfaces of galvanized steel panel joints. The first sample was for bolt spacing of 18 cm (3 bolts on test panel). A 7.5-cm wide strip normal to the joint between one or two sets of bolts increased the polarization by about a factor of three. However, a thin spacer in the joint, which required all panel-to-panel contact to be only by means of the 3 bolts, increased the leakage by a factor of 30.

Similarly, for bolt spacings of 7.5 and 9 cm (6 and 5 bolts, respectively, on the test panel) the plastic strip spacers between bolts increased the leakage by a factor of 3 to 4.

In the second group, several panel surface conditions were tested to determine the effect on leakage. The riveted aluminum van panels were painted, as normally done, on the outer surface and water sealed with caulking in the joint. This standard joint increased the leakage by about a factor of 5 over the nonpainted joint.

Hot rolled steel has a surface scale resulting from the rolling process. This scale increased the leakage over the leakage of a galvanized steel joint by a factor of 10. Removing this scale in the joint (wire brush and steel wool) decreased the leakage to within a factor of two of the galvanized steel joint.

Cold rolled steel panels were aged by rusting to determine the effects of rust in joints. The panels shown in Figure 10 were assembled after rusting. Rusted, nongalvanized steel joints obviously degraded the quality of the joint.

Joints cannot make continuous contact if the panels are not flat (smooth). Test panels were bent and then stamped flat to within 3 mm (one panel thickness), as shown in Figure 11. For these warped panels, the tests showed that if the fasteners were tight, the leakage was not affected by the warp in the panels. Apparently, the metal-to-metal contact at the ridges in the joint is sufficient to ensure an effective joint. Panels with the edges along the joint bent open increased the leakage by a factor of 3 apparently because of the decreased contact surface in the joint.

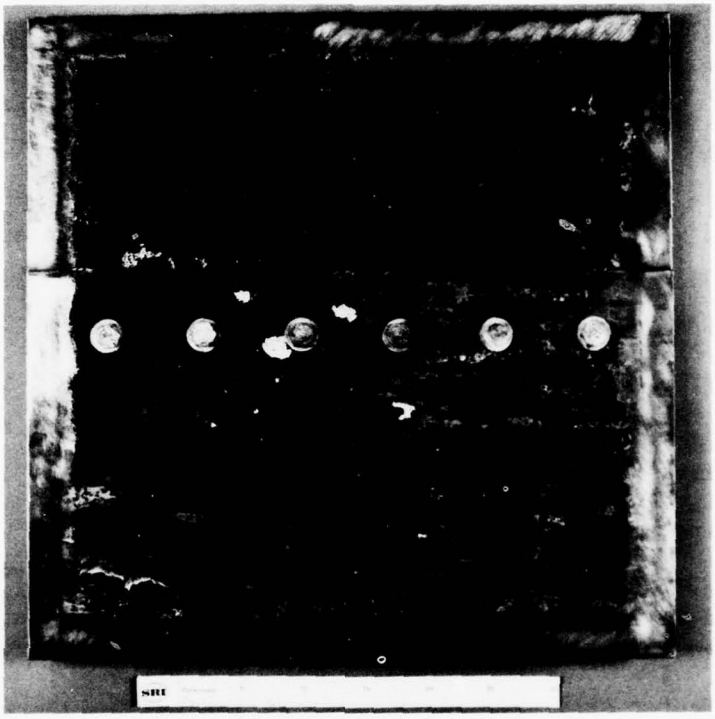

FIGURE 10 RUSTED STEEL PANELS

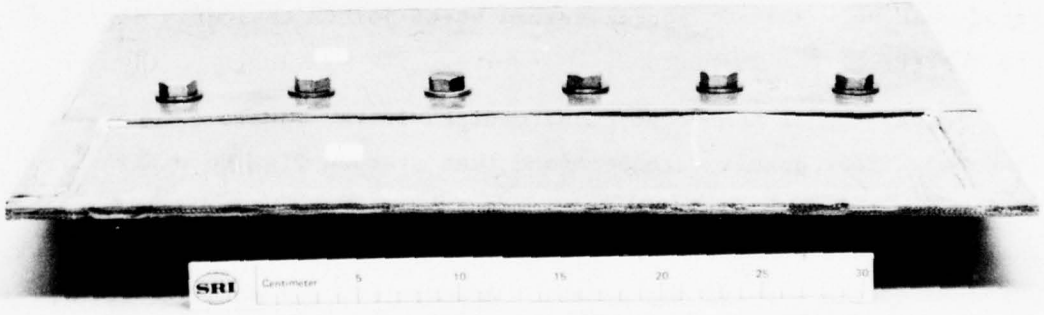

FIGURE 11 WARPED PANELS

The final group in Table 1 is concerned with joint hardware. Most panels were assembled with flat washers to apply maximum, uniform contact pressure to the joint. Lock washers, with their ability to penetrate surface scale, were tried and found to not be effective in reducing joint leakage.

Moisture leaks through joints can be reduced by the use of rubber washers under bolts and nuts and by the use of rope or ribbon caulking in the joint.[1] Each of these techniques only slightly effect joint leakage (a 50% increase).

The results of these tests indicated that the most important factor affecting leakage through joints is the quality of electrical contact between the mating surfaces of a joint. Paint, scale, and insulating films in the joint were the only factors tested that produced a significant change in the leakage. Degradations of 10 to 15 dB occurred when such contaminants were present in the joints. As indicated in Section II, however, joint leakage is also strongly dependent on fastener spacing; doubling the fastener spacing increases the leakage by 18 dB. Thus, for minimum leakage through a bolted or riveted shield, the bolt spacing should be small and the mating sheet-metal surfaces should be clean.

C. JOINT TREATMENTS

In this series of tests, various joint treatments were tested that might be proposed to improve the quality of the joint. These treatments included using conductive epoxy in the joint, placing copper tape between the mating surfaces, and tack welding along the joint. The results of these tests are summarized in Table 2.

The importance of panel metal-to-metal contact has already been discussed. Conductive epoxy potentially can provide this contact. The data in Table 2 indicate that if the metal-to-metal contact is good, as in the galvanized steel samples, putting conductive epoxy in the joint has little effect. If the joint is quite poor, as in the aluminum with sheet-metal screws or the steel with rust or scale, the conductive epoxy in the joint significantly decreases the leakage.

Table 2

JOINT TREATMENTS

	Panel Material	Joint	Problem	Polarizability ($m^3/m \times 10^{-6}$)
Conductive Epoxy	Galvanized steel	10-cm overlap 7.5-cm bolt spacing (6 bolts) 4 m-kg torque	1. Bent up edges 2. Conductive epoxy on edges 3. Epoxy fractured	0.29 0.31 0.23
	Galvanized steel	5-cm overlap 9-cm bolt spacing (5 bolts) 4 m-kg torque	1. None 2. Conductive epoxy in overlap	0.16* 0.08*
	Aluminum (sheet metal screws)	5-cm overlap 18-cm spacing	1. None 2. Conductive epoxy in overlap	10.4 0.08*
	Cold rolled steel (rusted)	10-cm overlap 7.5-cm bolt spacing (6 bolts) 4 m-kg torque	1. None 2. Conductive epoxy on edges 3. Conductive epoxy in overlap	186 184 2.8
	Hot rolled steel	10-cm overlap 7.5-cm bolt spacing (6 bolts) 4 m-kg torque	1. None 2. Conductive epoxy on edges 3. Conductive epoxy in overlap (cleaned)	9.9 2.6 3.1
Conductive Tape	Galvanized steel	10-cm overlap 7.5-cm bolt spacing (6 bolts) 4 m-kg torque	1. None 2. Copper foil in overlap	0.08* 0.53
Welding	Hot rolled steel	10-cm overlap 7.5-cm bolt spacing (6 bolts) 4 m-kg torque	1. None 2. One tackweld 3. Two tackwelds, one on each side	9.9 0.54 0.49
	Hot rolled steel	10-cm overlap 7.5-cm bolt spacing (6 bolts) 4 m-kg torque	1. None 2. Two tack welds 3. Four tack welds 4. Six tack welds 5. Eight tack welds 6. Ten tack welds 7. Seam welded	2.4 1.5 1.1 1.0 0.5 0.3 0.08*
	Galvanized steel	5-cm overlap	1. 30% seam weld	0.6

*This measurement is near the measurement threshold.

Although the conductive epoxy has much lower conductivity than the metals, it probably has little effect on the joint resistance of a good joint. However, conductive epoxy does fill the voids between the mating parts with lossy material through which leakage fields must penetrate. Thus, for leaky joints such as the rusty or scaly steel joints, the conductive epoxy provides an attenuating filter, as well as possibly improving the electrical contact.

One test was conducted with copper foil tape between the overlapped pieces of a bolted, galvanized steel joint. The foil tape was intended to provide copper surface-to-surface contact. The foil tape increased the leakage through the joint by a factor of 5. Subsequent tests on the foil tape determined that the adhesive was nonconducting, which provided poor foil tape to panel contact.

The remainder of the tests in this category involved adding tack welds to joints in steel panels. The first series of tests started with scaly panels that were quite leaky (polarizability 9.9×10^{6} m^3/m). Adding one tack weld reduced the leakage by a factor of over twenty. Adding a second tack weld on the other side of the panel had no significant effect.

On the 50-cm test sample, tests with more tack welds, ranging up to continuous welds, showed a continuous improvement with welding. These test measurements, near the sensitivity of system measurements, may not be indicative of the effects of welding. The 30% welds shown in Figure 12 are at least as effective a shield as a good bolted overlapping shield.

D. JOINT CHARACTERISTICS

The tests with tack welds on steel joints added insight about the parameters that affect joint leakage. In all cases, the bolted joints between hot-rolled plate indicated significantly greater leakage than comparable aluminum and galvanized steel joints; generally, the hot-rolled joints were comparable to the galvanized steel joints with a plastic sheet between the mating surfaces. Adding tack welds reduced the leakage, but not to the levels achieved with bolted aluminum or

FIGURE 12 PANELS WITH 30% WELDS

galvanized steel joints with similar fastener spacings. It appears, therefore, that the scale on the hot-rolled plate produced an insulating (or at least poorly conducting) layer between the mating surfaces that not only caused poor electrical contact, but also formed a large gap between the joined pieces through which the fields could penetrate. When this gap was filled with conductive epoxy, the leakage was reduced, but again, not to the levels achieved with clean aluminum or galvanized steel joints.

This effect of scale is illustrated in Figure 13. Note that the scale increased the effective width of the gap between fasteners and probably also increased the effective length of the gap. Because the leakage increases with the cube of the gap length, increasing the gap

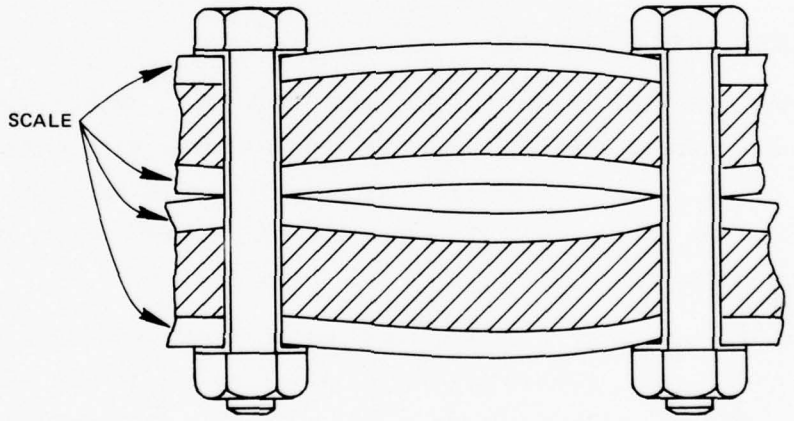

(a) JOINT WITH SCALE

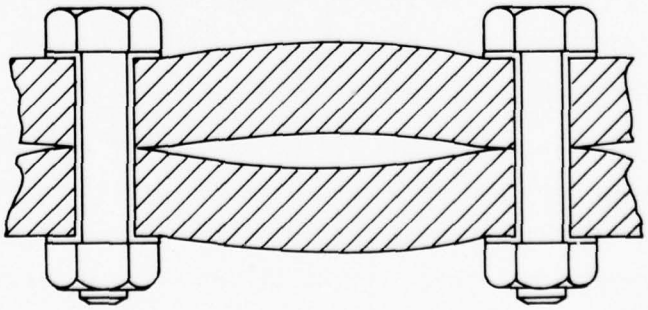

(b) WITHOUT SCALE

FIGURE 13 EFFECT OF SCALE IN THE GAP BETWEEN FASTENERS

length will cause serious degradation of the shielding effectiveness of the joint. Note that the scale prevented the bolt heads and nuts from making good contact with the base metal, so that the effective length of the gap may occasionally have been two or more bolt spacings. This may account for the wide variation of leakage from one sample to the rest, or from disassembly and reassembly of the same sample, that is apparent in the test data.

Although aluminum and zinc have insulating oxide surface films, these films are thin and the base metal is soft so the fasteners can break through the oxide to make metal-to-metal contact. The scale on hot-rolled steel is thick and hard, and the base metal is hard. Making metal-to-metal contact without removing the scale is, therefore, difficult with hot-rolled steel plate.

E. PATCHING SHIELD OPENINGS

Obvious openings in the shields will leak EMP. Methods to seal openings were tested that included covering openings with conductive materials. All except one involved the use of conductive epoxy; one involved the use of copper foil tape. The results of the tests are summarized in Table 3.

Tests on open slots or holes in aluminum sheet were used for the "before patch" leaks. These are very leaky compared to the bolted joints, as evidenced by the polarizations of over 100×10^{-6}, compared to less than 10×10^{-6} for the worst bolted joints. For copper foil tape placed over the array of 3 slots, the leakage was reduced by almost 34 dB, but it is significant that the leakage was still greater than the leakage through any of the bolted or riveted joints.

For the tests in Table 3, the open holes were covered on one side with masking tape and then coated on the other side with conductive epoxy. In each case, a marked reduction leakage (over 20 dB) was observed, but the remaining leakage was still moderate to large.

Table 3

JOINT PATCHING

Material	Joint	Patch	Polarizability ($m^3/m \times 10^{-6}$)
Aluminum (1 mm)	10-cm hole	1. None	175
		2. Sealed with conductive epoxy	9
Aluminum (1 mm)	7.5-cm slots (three)	1. None	566
		2. Copper foil tape, both sides	12
Aluminum (1 mm)	7.5-cm slot (one)	1. None	275
		2. Sealed with conductive epoxy	1.2
Aluminum (3 mm)	7.5-cm slots (three)	1. None	566
		2. 10-cm overlap	5.3

F. JOINT LEAKAGE SUMMARY

Tests have demonstrated that the two most important factors affecting the leakage at overlapped joints in sheet metal are (1) the quality of contact (between the sheet metal panels and between the fasteners and the sheet metal) and (2) the amount of gap between the jointed parts caused by bowing out or by foreign material (scale, rust, paint, or other). The effect of contact was demonstrated by the tack-weld tests on hot-rolled sheet. The tack-welds consistently improved the leakage-resistance of the joint even though the scale remained. A more dramatic improvement occurred when the scale, rust, paint, or simulated coating (plastic film) was removed from the mating surfaces. Improvement by factors of five (or more) were realized by cleaning the mating surfaces so that metal-to-metal contact was possible. This apparently reduced the effective size of the gap between mating parts as well as increased the electrical conductivity between the parts.

Cleaning the mating surfaces also increased the probability that the bolts (or other fasteners) would make contact with the sheet metal. Bolt contact is important, particularly if sheet metal contact is poor,

because without bolt contact the gap between joined parts may not be broken up into a series of short gaps. In view of the cubic dependence of leakage on gap length, it became evident that failure to make good contact at each fastener results in serious degradation of the shield quality at the joint.

IV JOINT LEAKAGE EFFECTS ON SHIELDING

A. SHIELDING CHARACTERISTICS

The shielding requirements for continuous, welded sheet-metal liners can be satisfied by 1 mm of mild steel (greater than 60 dB for frequencies above 10 kHz). A continuous steel liner will satisfy the requirements for low frequency EMP shielding and will exceed the higher frequency shielding requirements (typically 80 to 100 dB). Overlapping bolted joints will leak EMP energies at higher frequencies and may not meet the high frequency requirement.

The effect on shielding of bolted joint leakage at higher EMP frequencies can be estimated for a structure, such as the aircraft shelter shown in Figure 1 and in Figure 14(a) by modeling the structure as a cylinder of the same circumference as shown in Figure 14(b). The effects on shielding are calculated as the voltage induced on a wire on the axis of the cylinder from the polarizability of the joints and the current induced on the outer surface of the cylinder by the EMP fields. For comparison, the voltage induced on the internal wire by diffusion of the magnetic field through 1 mm of mild steel is also calculated.

Also, for a wire close to the wall of the shelter, it was felt that the wire-and-plane model of Figure 14(c) might give a better approximation of the induced voltage. Therefore this model was also used to estimate the induced voltage on an internal conductor.

B. LEAKAGE INDUCTANCE

In either the coaxial model or the wire-and-plane model, some of the joints are parallel to the direction of the external current, and some are perpendicular to the current direction. Measurements of the polarizability of several joints were made for both directions of current flow relative to the direction of the seam to evaluate the effect of current flow parallel to the joint. The results of these measurements

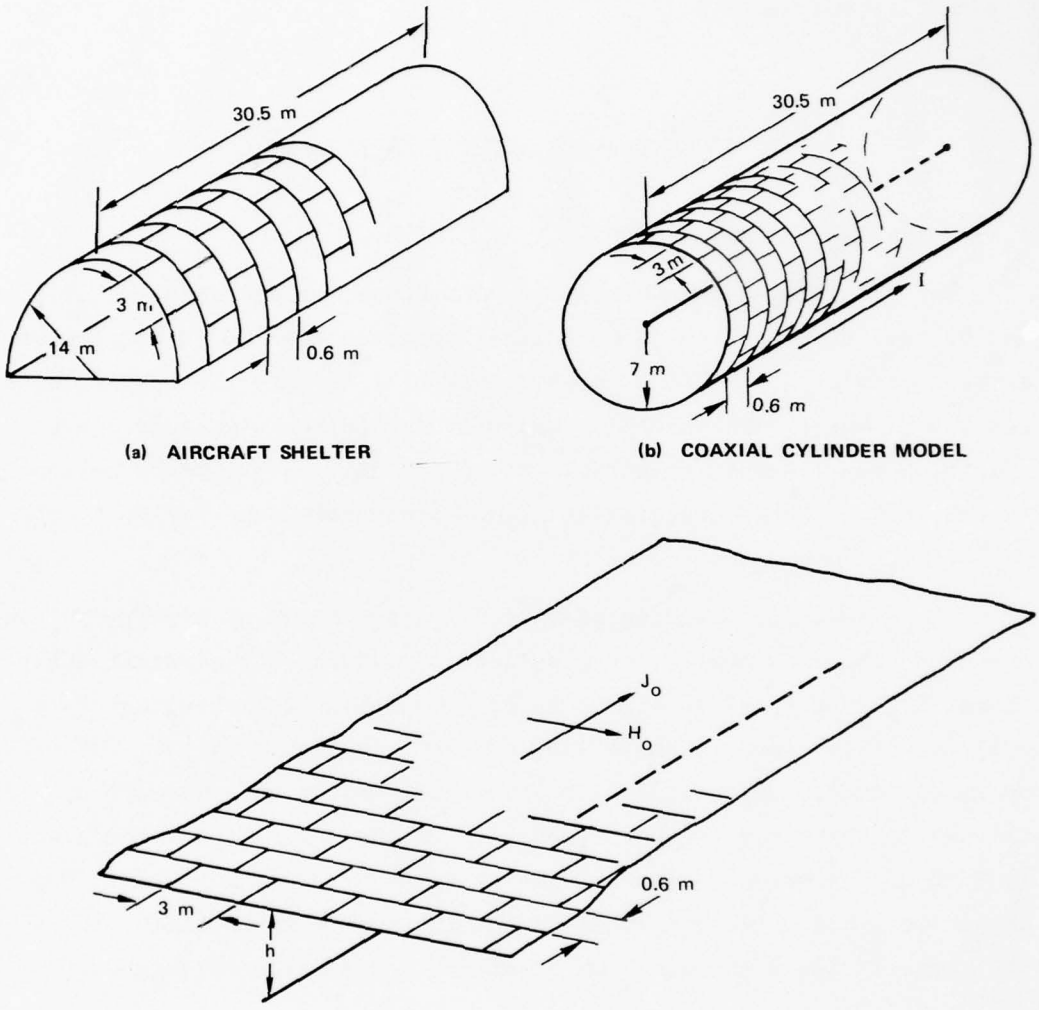

(a) AIRCRAFT SHELTER

(b) COAXIAL CYLINDER MODEL

(c) WIRE-AND-PLANE MODEL

FIGURE 14 MODELS FOR ANALYZING JOINT LEAKAGE IN AN AIRCRAFT SHELTER

are given in Table 4. It can be seen from the table that the polarizability per unit length of joint for current flow parallel to the seam is roughly one tenth as large as it is for current perpendicular to the seam. Because of this, the leakage through the circumferential seams is much larger than the leakage through the axial seams when the current in the shelter flows in the axial direction. In addition, there is about five times as much circumferential joint per unit length of shelter as

Table 4

MEASURED POLARIZABILITIES FOR CURRENT PERPENDICULAR TO AND PARALLEL TO A SEAM

Configuration	Polarizability ($m^3/m \times 10^{-6}$)	Remarks
Aluminum sheet, 3-in. lap, 2 rows of rivets staggered	1.1 perpendicular 0.064 parallel	ratio: 0.058
Galvanized steel, 2-in. lap, 30% weld both sides	0.58 perpendicular 0.079 parallel	ratio: 0.14
Aluminum sheet, slot covered with conductive coating	1.2 perpendicular 0.078 parallel	ratio: 0.066

there is axial joint. This relation can be shown by considering the dimensions of the shelter and its panels shown in Figure 14. For each meter of shelter length in the axial direction, there is $14\pi/3 = 14.7$ meters of axial joint and $14\pi/0.6 = 73.3$ meters of circumferential joint. Because of these factors, the leakage through axially directed joints has been neglected.

For the coaxial cylinder model, the leakage inductance is given, in Henrys, by[5]

$$M = \frac{\mu_o}{4\pi^2 a^2} \left(\frac{2\pi a}{0.6}\, m\right) \quad , \tag{9}$$

where μ_o is the permeability of air, a is the radius of the cylinder, $(2\pi a/0.6)$ is the length of joint per meter of cylinder, and m is the polarizability per unit length of the joint as measured in the rectangular coaxial tester described in Section II. The leakage inductance, M, relates the voltage, V, induced per meter of internal conductor to the rate of change of the current on the cylinder in volts per meter as:

$$V = M \frac{di_o}{dt} \quad . \tag{10}$$

For the wire-and-plane model, the voltage increment induced in the wire by an increment of linear aperture (see Figure 15) is[6]

$$dV_1 = \mu_o m dx \frac{h}{\pi(x^2 + h^2)} \frac{dH_o}{dt} \quad . \tag{11}$$

By integration with respect to x, the voltage induced by a single long joint ($x \rightarrow \pm\infty$) is

$$V_1 = \mu_o M \frac{dH_o}{dt} \quad . \tag{12}$$

Since $H_o = i_o/2\pi a$ for an excitation of the plane equivalent to the excitation of the cylinder by the current i_o, and since there is one aperture (joint) every 0.6 m, the induced voltage per unit length is

$$V = \frac{\mu_o M}{2\pi a(0.6)} \frac{di_o}{dt} \tag{13}$$

or

$$M = \frac{\mu_o M}{2\pi a(0.6)} \quad , \tag{14}$$

which is the same for the coaxial cylinder model.

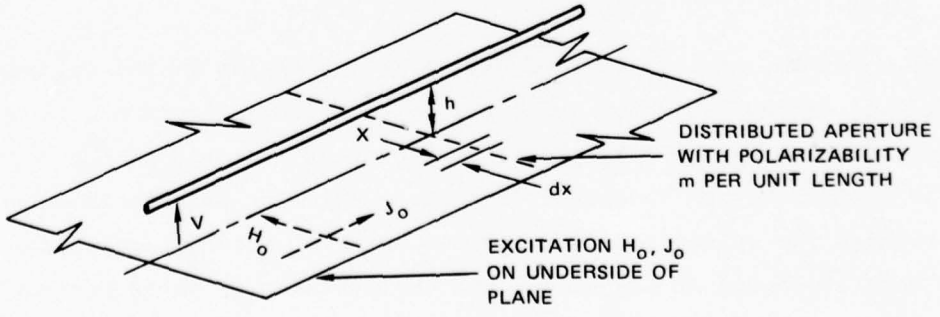

FIGURE 15 WIRE-AND-PLANE CONFIGURATION WITH DISTRIBUTED APERTURES

In either model, it is postulated that the cross section (radius a in the coaxial model; h in the wire-and-plane model) is small compared to the wavelength of the exciting current. Because of the large dimensions of the aircraft shelter, this postulate does not hold at the high frequencies in the EMP spectrum. However, experience with coupling to overhead power lines has demonstrated that the error incurred in violation of this postulate is small (15 to 20%), even when a or h are equal to a few wavelengths.[7] Furthermore, for buried structures, the higher frequencies are substantially attenuated by the soil, so that they are not dominant excitation sources for these structures.

C. VOLTAGE INDUCED ON AN INTERNAL WIRE

The voltage induced per meter of internal wire (parallel to the direction of the current in the shelter) is

$$V(\omega) = Z_T I_o(\omega) \quad , \tag{15}$$

where Z_T is the transfer impedance of the shelter wall and $I_o(\omega)$ is the current induced in the shelter wall by the EMP. The transfer impedance is[8]

$$Z_T = R_o \frac{\gamma T}{\text{Sinh } \gamma T} + j\omega M \quad , \tag{16}$$

in which R_o is the direct current resistance per unit length of the walls, γ is the complex propagation factor for the wall steel, T is the wall thickness, and M is the leakage inductance of the joints between wall panels. The resistance R_o and propagation factor γ are given by

$$R_o = \frac{1}{2\pi a \sigma T} \tag{17}$$

and

$$\gamma = (1 + j) \sqrt{\pi f \mu \sigma} \quad , \tag{18}$$

where σ is the conductivity of the steel, μ is the permeability of the steel, f is the frequency in Hertz ($\omega = 2\pi f$), and $j = \sqrt{-1}$. For $\sigma = 6 \times 10^6$ mho/m, $\mu = 100\ \mu_o$, and T = 1 mm, the resistance in ohms per meter is:

$$R_o = 3.79 \times 10^{-6} \quad , \tag{19}$$

and $T\sqrt{\pi f \mu \sigma} = 1$ when f = 422 Hz. These factors determine the diffusion through the walls.

For a typical joint with a polarizability of 10^{-6} m^3/m, the leakage inductance in Henrys per meter is

$$M = 4.76 \times 10^{-14} \quad . \tag{20}$$

A plot of the transfer impedance $Z_T = V(\omega)/I(\omega)$ is shown in Figure 16 for these values of R_o, M, and μ. Also shown is the magnitude of $j\omega M$

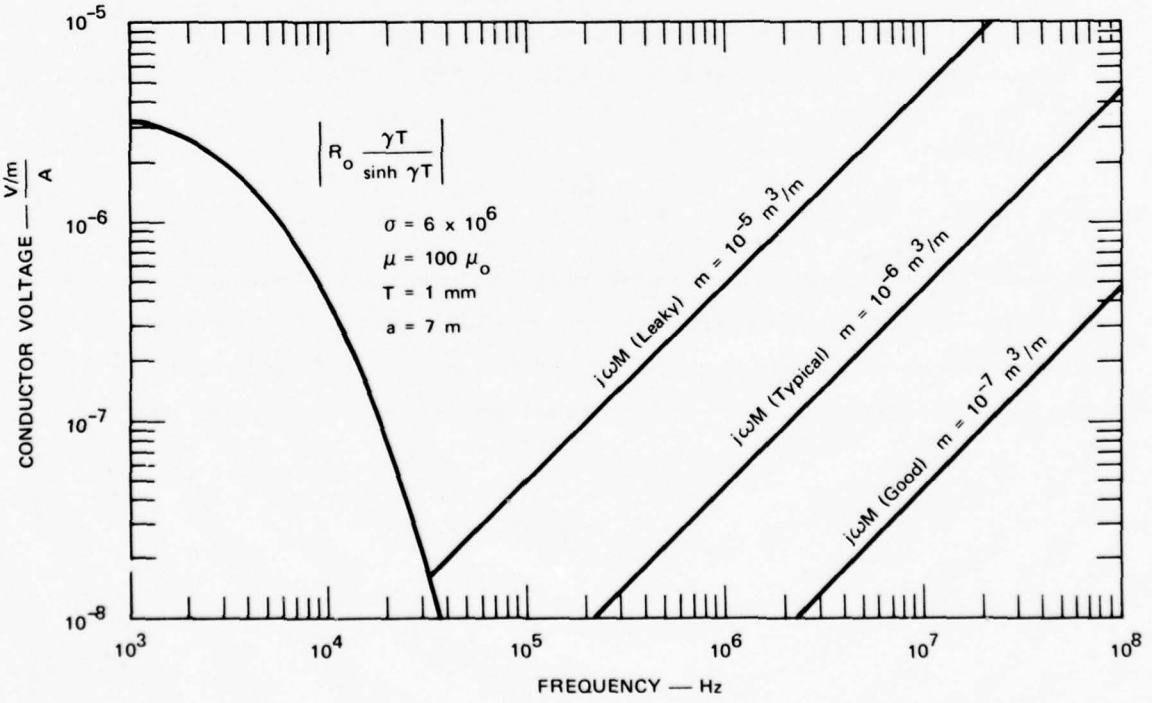

FIGURE 16 INDUCED VOLTAGE PER UNIT LENGTH OF INTERNAL WIRE PER AMPERE OF SHIELD CURRENT

for leaky, typical, and good joints with a polarizability of 10^{-5}, 10^{-6}, and 10^{-7} m^3/m respectively.

The current $I_o(\omega)$ in the shelter wall is assumed to be

$$I_o(\omega) \approx 2\pi a\, H_o(\omega) \tag{21}$$

$$\approx 4\pi a\, H_{inc}(\omega) \quad , \tag{22}$$

where $H_o(\omega)$ is the outside surface magnetic field strength and $H_{inc}(\omega)$ is the incident field strength. This assumption is equivalent to postulating that the current is uniformly distributed about the girth of the shelter and that the surface field is twice the incident field. The first postulate is a good approximation at low frequencies ($a \ll \lambda$, where λ is the wavelength), but it provides an overestimate of the excitation at high frequencies where the current on the "shadow" side is smaller than that on the side facing the source. The second postulate is good at high frequencies ($a \gg \lambda$), but it gives low estimate of the excitation at the low frequencies where diffusion is important. Because our purpose here is to compare the leakage through joints with the leakage through a seamless shield, however, these postulates are conservative in that they make the joint leakage appear to be somewhat worse (in comparison to the diffusion) than it actually is.

The magnetic fields of the high-altitude EMP at the surface and at 10 and 20 meters below the surface are shown in Appendix B and in Figure 17 for an angle of incidence of 70° from vertical and a horizontally polarized incident wave (i.e., the electric vector is horizontal). These fields were derived for an incident wave of the form

$$H(t) = \frac{E_o}{\eta} \left(1 - e^{-t/t_1}\right) e^{-t/t_2} \quad , \tag{23}$$

where E_o = 50 kV/m, t_1 = 3.5 ns, t_2 = 275 ns, and $\eta = 120\pi$. Also shown in Figure 17 are the electric field incident on the surface of the earth and the electric field in the soil.

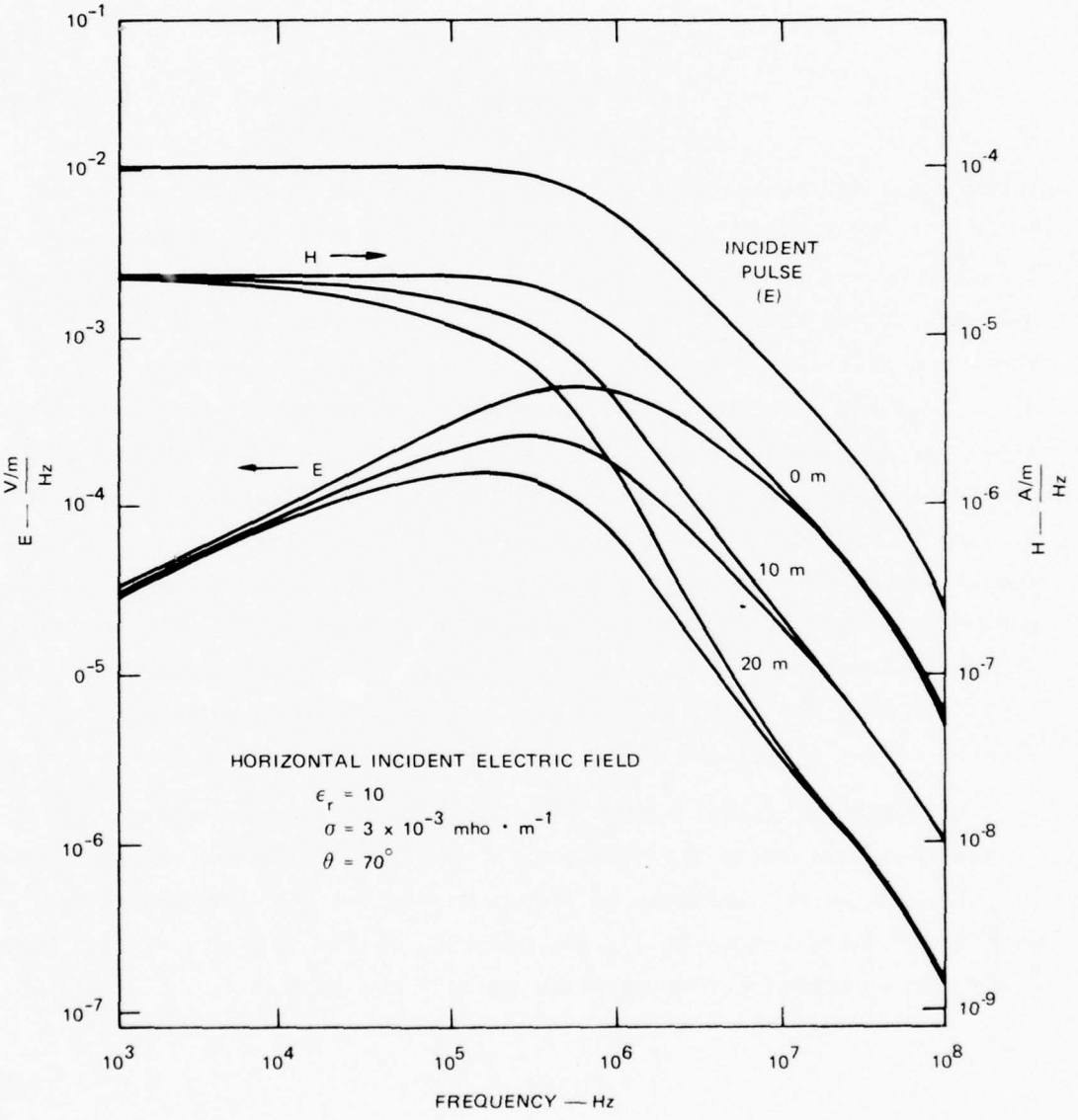

FIGURE 17 SPECTRA OF ELECTRIC AND MAGNETIC FIELDS AT VARIOUS DEPTHS

The spectrum of the voltage induced in each meter of wire inside the shelter by the magnetic field of the EMP is shown in Figure 18 for a surface shelter and for a shelter 20 meters underground. Also shown here are the 60 and 80 dB shielding levels. The induced voltage spectrum for both the typical joint ($m = 10^{-6}$) and the leaky joint ($m = 10^{-5}$) for a surface shelter are shown for the high frequencies.

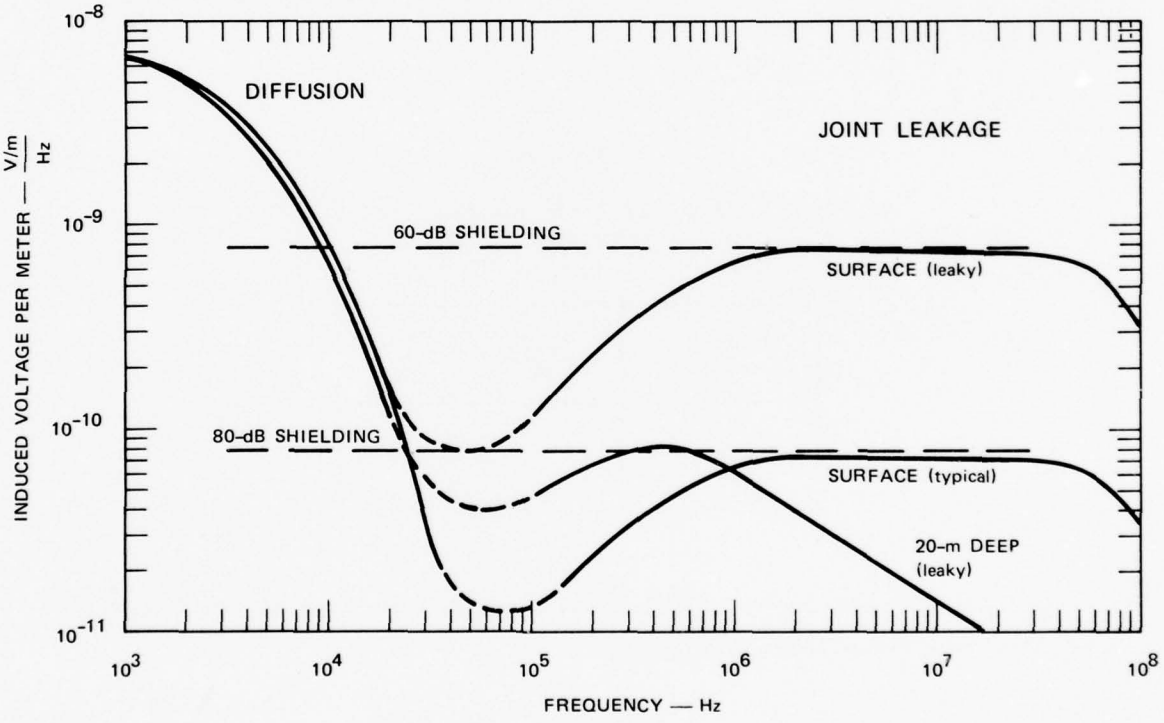

FIGURE 18 VOLTAGE SPECTRUM INDUCED BY THE HIGH ALTITUDE EMP

In the time domain, the voltage induced on the internal wire is

$$V = M \frac{di_o}{dt} \tag{24}$$

and

$$I_o \approx 4\pi a H_o \quad .$$

Using the two exponential form of the EMP field, the maximum rate of change of the current in amperes per second in the shelter walls occurs at t = 0 and is

$$\frac{di_o}{dt} = 4\pi a \frac{E_o}{\eta}\left(\frac{t_2 - t_1}{t_1 t_2}\right) = 3.33 \times 10^{12} \quad . \tag{25}$$

For this model, Appendix B shows that the ratio of the below-ground rate of rise to that of the incident field decreases with depth of burial, as indicated in Table 5.

Table 5

MAXIMUM RATE-OF-RISE OF THE MAGNETIC FIELD WITH DEPTH IN THE SOIL

Depth d (m)	$\frac{dH(d)}{dt} \Big/ \frac{dH_{inc}}{dt}$
0	0.174
10	0.029
20	0.005

Thus the peak voltage (per meter of wire) induced in the internal wire by the joint leakage field is

$$V_{peak} = 3.33 \times 10^{12} \, M = 0.16 \tag{26}$$

for an above-ground shelter and 1/200th as much (0.8×10^{-3}) for a shelter 20 meters below-ground. Sketches of the induced waveforms on a wire in an above-ground shelter and at various depths of burial are shown in Figure 19(a). (These sketches were made from calculated values of the positive and negative peaks and times of peaks and zero crossings assuming the typical joint leakage--$m = 10^{-6}$.)

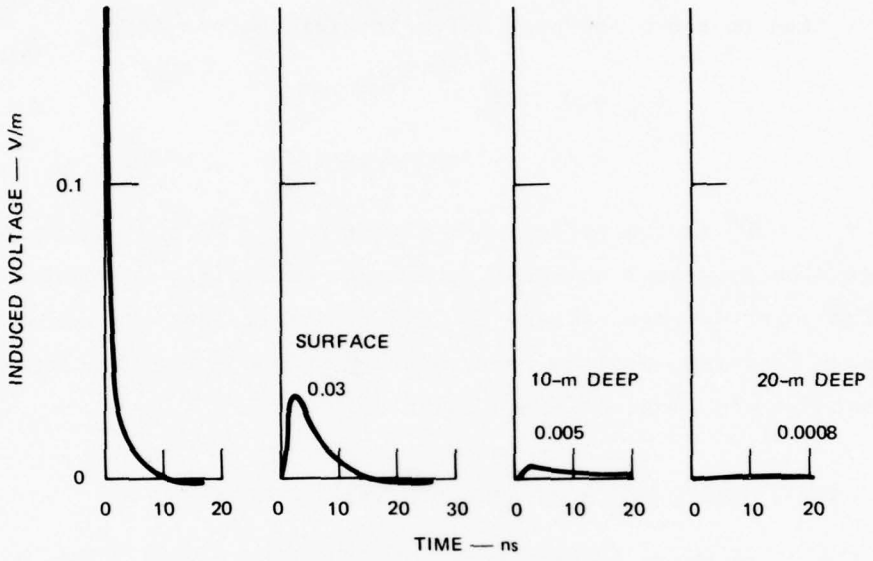

(a) JOINT LEAKAGE

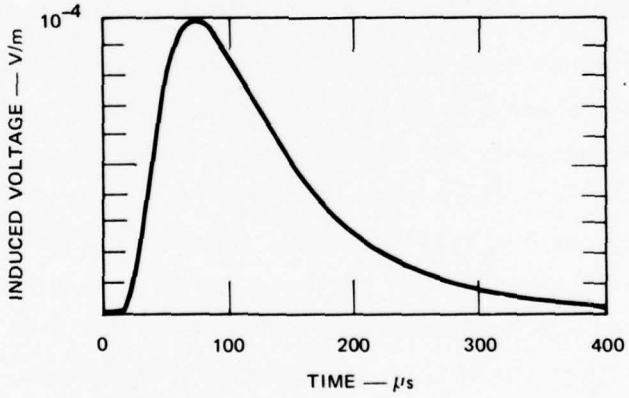

(b) DIFFUSION THROUGH WALLS (above ground)

FIGURE 19 VOLTAGE WAVEFORMS INDUCED ON INTERNAL WIRE

Figure 19(b) shows the waveform of the voltage induced by the magnetic field that diffuses through 1 mm steel walls. This waveform is the impulse response of the shielded conductor. Its peak value in volts per meter of conductor is[8]

$$V_{pk} = 5.9\ R_o \frac{\tau}{\tau_s} (4\pi a\ H_{pk})$$

$$= 9.5 \times 10^{-5} \qquad \text{(above-ground)} \quad , \qquad (27)$$

and the time to reach the peak value in microseconds is

$$t_{pk} = 0.09\ \tau_s$$
$$= 78 \qquad \text{(above-ground)} \quad , \tag{28}$$

where $\tau_s = \mu\sigma T^2$ is the diffusion constant of the shield. This induced voltage also decreases somewhat with depth of burial, but much less so than the joint leakage because the low frequency spectrum dominates the diffusion response, and the low frequency magnetic field is only slightly attenuated as is apparent from Figure 17.

D. LEAKAGE MEASUREMENTS ON AIRCRAFT SHELTER PANELS

Five sections of the aircraft shelter liner panels shown in Figures 1 and 2 were assembled and tested to measure joint leakage. These panels have fastener (bolt) spacings of 15 cm with a joint overlap of 11 cm.

Two measurements were made to establish joint characteristics. Figure 20 shows a transient source and transmission line coupling network that couples current onto the liner. This current is shown in Figure 21(a). With the joint opened, the current on the inner surface [Figure 21(b)] shows the rate of change dependence before the measurement setup interference arrives from the panel edges. Figure 21(c) shows this inner current for the panels bolted with a torque of 4 m-kg. The joint leakage is less than the shielding measurement threshold.

The second test on the liner panels measured the joint resistance R_j shown in Figure 3(a). This measurement was made by applying a direct current voltage to the five panels shown in Figure 20 and measuring the voltage drop across each joint. The voltage drop across the joint was 3.3 times that measured on an equal distance on the panels, which indicates that the bolted joints (11 cm overlap with 15 cm bolt spacing) provide metal-to-metal contact nearly equal to that of continuous panels. Measurements on panel joints with hand-tight bolts increased the joint contact resistance by about 5%. The zinc-coated, curved panels apparently make good contact with a minimum of bolt torque.

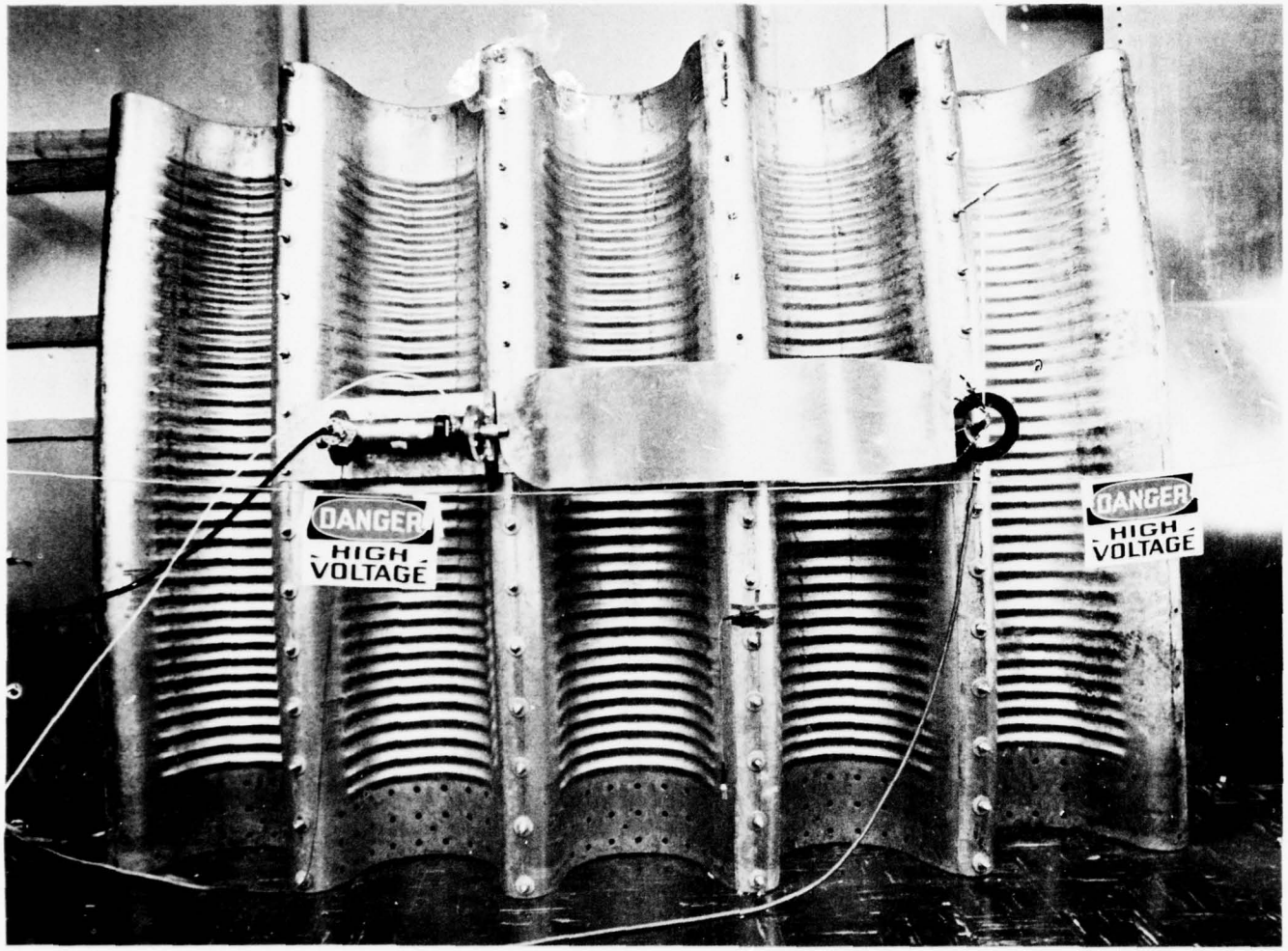

FIGURE 20 AIRCRAFT SHELTER TEST PANELS

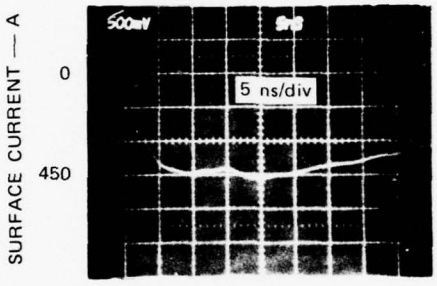

(a) DRIVING TRANSIENT

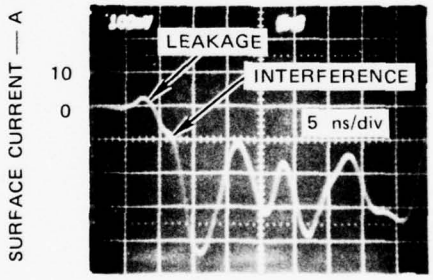

(b) OPEN JOINT

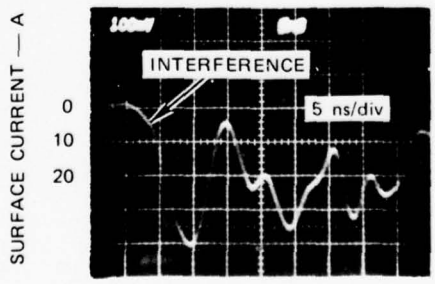

(c) BOLTED JOINT

FIGURE 21 TRANSIENT TEST DATA

E. INTERPRETATION OF RESULTS

The attenuation as a function of frequency shows that the leakage through joints is lower than the diffusion at 10 kHz (60 dB of shielding) through 1 mm of steel at all EMP frequencies. If the joints are typical ($m = 10^{-6}$) or good ($m = 10^{-7}$) or if additional shielding equivalent to 20 m of earth are provided, then the high frequency leakage is always less than 80 dB of shielding.

The voltage waveforms induced on the internal conductor show that the peak voltage induced on an internal wire from joint leakage is much larger than the peak voltage induced by the diffused magnetic field. There are several considerations, in addition to the pessimistic assumptions regarding the shield current, that affect any conclusions drawn from the time dependent results. These are:

(1) The integrated voltage-time impulse ($\int v dt$) for the diffused pulse in Figure 19(b) is much greater than the comparable pulse induced by joint leakage. This is true even if the "leaky" joint ($m = 10^{-5}$) is used for a surface shelter liner. Thus, the diffused pulse contains much more energy than the joint-leakage pulse.

(2) The slow, diffused pulse is cumulative along a long wire; the very short joint leakage pulse is much less cumulative. Thus, for example, a 30-meter-long axial wire would have 30 times the voltage induced into one meter of wire by the diffused field. For the EMP incident at broadside to the shelter (the condition that induces maximum current in the shield walls), the joint-leakage voltage induced in a long wire is of the order of $c\tau$ times the voltage induced in one meter of wire (c is the speed of light, τ is the pulse width). Thus, for the very short pulses ($\tau \sim 10^{-8}$ s) induced through joint leakage, the voltage in a long wire is only about a factor of three greater than the per unit length values shown in Figure 19(a).

(3) Stray inductance and capacitance in wiring significantly attenuate the peak voltage or current induced by the joint leakage because of the large L di/dt voltage drops and C dv/dt current losses. Conductor and dielectric losses also attenuate such short pulses. Because of these factors, these transients do not propagate along the facility wiring as freely as the slow, diffusion-induced transients but can weakly couple to other cables.

V CONCLUSIONS AND RECOMMENDATIONS

A. SHIELDING PROPERTIES OF BOLTED JOINTS

The results of leakage measurements on joints indicate that the bolted sheet metal aircraft shelter liner shown in Figure 1 provides sufficient shielding to limit the voltage induced on long internal conductors by the high-altitude EMP to about 5 volts for "leaky" joints ($m = 10^{-5}$) or about 0.05 volts for "good" joints ($m = 10^{-7}$). The "leaky" joints were generally those with large bolt spacings (over 20 cm), small overlap (less than 10 cm), and poor mating surfaces (rust, scale, paint, or other foreign matter in the joints). The "good" joints are characterized, by metal-to-metal contact, clean mating surfaces, small bolt spacing (less than 10 cm) and overlap of at least 10 cm.

The important joint properties that control the shielding effectiveness are: sheet-metal to sheet-metal contact, and bolt-to-sheet-metal contact along the bolt line. This contact can be obtained with fastener contact pressure (3 to 4 kg-m of bolt torque) and clean sheet metal surfaces such as aluminum, copper, or galvanized steel. Surfaces with scale, such as hot rolled steel, do not make good metal-to-metal contact. Conductive epoxy in the joint will improve leaky joints.

Rope caulking (3 mm) or other insulating material does not degrade the bolt-line electrical contact and does not appreciably compromise the shielding characteristics of the joint provided these compounds are applied along one edge of the overlapped joint and not along the bolt line.

An aircraft shelter liner exposed to a high-altitude EMP will provide the equivalent of 60 dB of shielding with leaky joints ($m = 10^{-5}$) for all EMP frequencies (see Figure 18). Typical joints ($m = 10^{-6}$) and good joints ($m = 10^{-7}$) will provide 80 and 100 dB, respectively. In addition, the shelter liner is normally covered with about 0.5 m of concrete (steel

reinforced). This concrete cover will attenuate the maximum rate of rise of the EMP and subsequently attenuate the leakage signal by 6 to 10 dB.

Earth cover will also attenuate the EMP spectrum by about 1.5 dB per meter (see Figure 17), providing the equivalent of 80 dB shielding for leaky joints ($m = 10^{-5}$) at a burial depth of 20 m (see Figure 18). Twenty meters of earth cover also decreases the maximum rise of EMP (see Table 5), resulting in a 46 dB decrease in the joint leakage signal on long internal cables.

Although the very short, 5-volt signal caused by EMP-induced transients on internal wiring of the "leaky" bolted joints is comparable to the operating voltages of many electronic circuits, it is smaller than the transients normally present in a facility because of eminations from station-keeping equipment and operational electronic equipment. Thus, equipment that can tolerate the normal facility environment should not be adversely affected by the EMP-induced transients that penetrate the bolted sheet-metal shield.

The preceding conclusion is based on the assumption of a balanced protection system in which the first level of shielding (i.e., the building shield) is used to limit externally generated interference to levels comparable to equipment eminations or other internally generated interference. The second (equipment cabinet and framework) level of shielding is used to reduce this room environment to a level that small-signal electronic circuits can tolerate without malfunctioning. Obviously, if there is no secondary protection between the building shield and the small signal electronic circuits, the 5-volt EMP-induced transient for leaky joints may be troublesome.

B. JOINT CORROSION

The one aspect of the bolted sheet-metal shield problem that has not been adequately resolved by tests is the "life-cycle" quality of bolted joints. The effects of aging, corrosion, temperature cycling, and maintenance practices, on the effectiveness of the shield throughout its expected life are difficult to assess from a short-term series

of laboratory experiments. Good joints ($m = 10^{-7}$) were achieved using galvanized steel sheets; rusted nongalvanized-steel sheets (see Figure 19) resulted in a leaky joint ($m = 10^{-5}$). Hot-rolled steel with scale simulating surface corrosion resulted in a typical joint ($m = 10^{-6}$).

The results of the tests conducted to simulate some of the anticipated effects of aging indicate that the important properties to maintain are metal-to-metal and bolt-to-metal contact along the joints. How, or whether, this contact can be maintained throughout the life of the facility has not been demonstrated. However, it is likely that the solution to this problem (e.g., assembly quality control and corrosion preventing sealants) is more easily accomplished than the proof of its effectiveness.

C. AIRCRAFT SHELTER LINER APPLICATION

Bolted overlapped joints can provide the equivalent of 80 dB of shielding if the joint is effectively a typical joint ($m = 10^{-6}$). Good joints ($m = 10^{-7}$ and 100 dB of shielding) can be made by using clean sheet metals that make metal-to-metal contact (galvanized steel, aluminum, and copper). For the galvanized-steel aircraft shelter liner, joints should be made with a minimum overlap of 10 cm and with bolts torqued to 3 to 4 kg-m on spacings no larger than 7.5 cm to ensure a good joint ($m = 10^{-7}$). Metal-to-metal contact can be achieved by cleaning the surfaces with a solvant and inspecting for proper bolt torque during assembly.

The life-cycle quality of the joint can be improved with a waterproof mastik seal over the outer bolts and bolt holes and joint edge. By starting with a good joint ($m = 10^{-7}$) that gives the equivalent of 100 dB of shielding and by the additional shielding provided by concrete and earth covers, a moisture sealed joint is not expected to deteriorate more than an order of magnitude, resulting in a minimum of 80 dB of shielding for a liner fully exposed to EMP.

The bolted liner joints are only a part of the effectiveness of the aircraft shelter liner as an EMP shield. To achieve effective

shielding, the ends and floor of the shelter must be made of steel that can be continuous welded at all joints. Bolted overlap joints as described above may also be used if care is taken to ensure metal-to-metal contact, bolt torque, joint overlap, bolt spacing, and moisture sealing. Special attachment parts may be required to attach the arched panels to the floor and end walls.

VI REFERENCES

1. "Instructions for Assembly and Erection of 100-foot Long Steel Arch Aircraft Shelters Type A," Marwais Steel Company, Richmond, California (15 July 1970).

2. C. G. Montgomery et al., Principles of Microwave Circuits, p. 178 (Dover Publications, New York, 1965).

3. E. F. Vance and W. C. Wadsworth, "Rectangular Coaxial Skin Tester," Technical Memorandum 24, Contract F29601-69-C-0127, SRI Project 7995, Stanford Research Institute, Menlo Park, California (September 1973).

4. "EMP Protection for Project 85, Executive Summary," Illinois Institute of Technology Research Institute, Chicago, Illinois (April 1975).

5. N. Marcuvitz, Waveguide Handbook, MIT Radiation Laboratory Series, Vol. 10 (McGraw-Hill Book Company, New York, 1951).

6. D. Kajfez, "Excitation of a Terminated TEM Transmission Line Through a Small Aperture," Interaction Note 215, Air Force Weapons Laboratory, Kirtland AFB, New Mexico (July 1974).

7. W. E. Scharfman and E. F. Vance, "EMP Coupling and Propagation to Power Lines: Theory and Experiments," Technical Report 8, Contract F29601-69-C-0127, SRI Project 7995, Stanford Research Institute, California (May 1973).

8. E. F. Vance, "Coupling to Cables," DNA 2114, Chapter 11 (revised), Defense Nuclear Agency, Washington, D.C. (December 1974).

Appendix A

Abstracted from Reference 3

RECTANGULAR COAXIAL SKINTESTER

by

E. F. Vance and W. C. Wadsworth

September 1973

Appendix A

Abstracted from Reference 3

RECTANGULAR COAXIAL SKINTESTER

Description of Tester

The skin-joint tester operates on the principle of an iris-coupled coaxial-transmission-line coupler. The test panel containing the leaky joint or access door is made into a common wall shared by two rectangular coaxial transmission lines. The larger transmission line is driven by passing power from a CW source through the rectangular transmission line to a matched load. The smaller rectangular transmission line, which is coupled to the driving line through only the test panel, is terminated in its characteristic impedance at one end and connected to instrumentation for measuring the coupled power (voltage or current) at the opposite end. Since the power coupled to the second (sensing) line is proportional to the power through the driving line and the leak characteristics of the test panel, a measure of the coupled power is a measure of the leak characteristic of the test panel.

The skin-test facility was designed for test panels approximately 0.5 m square. The test panel is mounted in a window in the wide wall of the outer conductor of the rectangular coaxial transmission line used to carry the excitation power. The outer conductor of the sensing line also has a framed window in its wide wall. This window nests inside the frame of the window in the drive line so that the window in the sensing line encloses only the test panel, and the junction of the test panel with the driving line is not included in the sensing line (see Figures 1 and 2). Both the sensing line and the driving line are symmetrical so that the driving line can be driven from either end and the power coupled to the sensing line can be measured at either end. This symmetrical construction permits directional effects associated with a combination

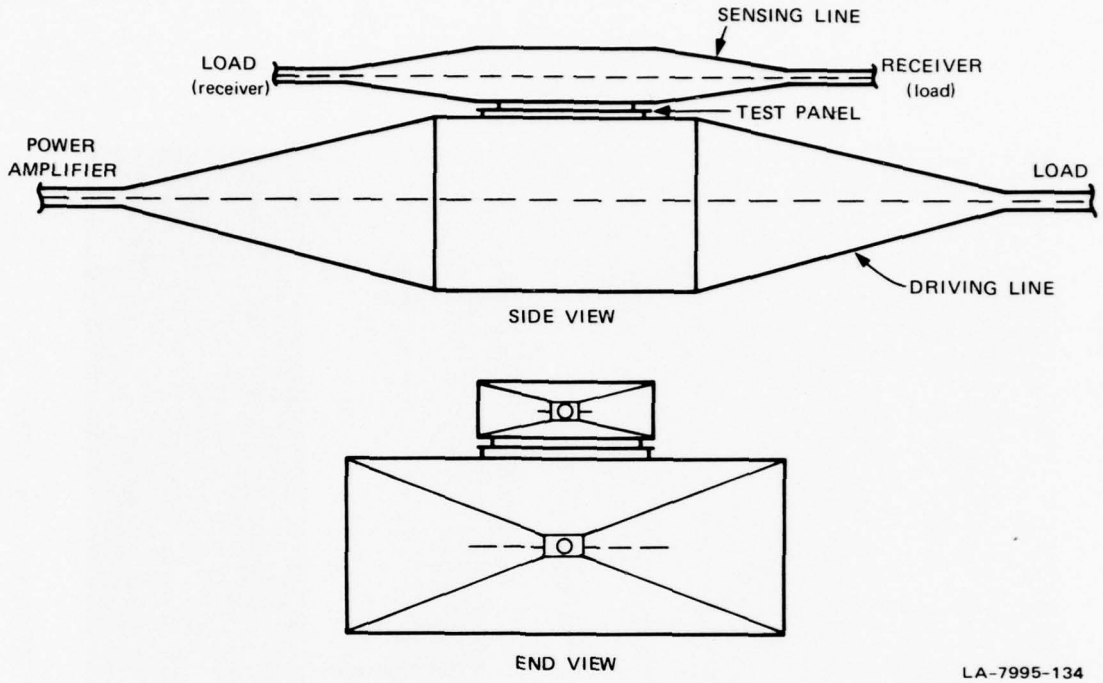

FIGURE A-1 SKETCH OF RECTANGULAR COAXIAL-TRANSMISSION-LINE SKIN TESTER

of electric and magnetic coupling to be studied. It also permits push-pull excitation schemes to be used, if desired. Both the sensing line and the driving line are 50-ohm structures throughout the 10-kHz-to-100-MHz test frequency range.

The driving line is provided with electric- and magnetic-field sensors installed in the wall opposite the test panel. These sensors have been calibrated in terms of the electric and magnetic fields, respectively, and in terms of the voltage applied to the driving line. These sensors can therefore be used to measure the excitation level for the test panel.

B. Theory of Operation

As indicated above, the skin tester operates on the principle of an iris-coupled transmission-line coupler. The coupling iris, which is the skin joint or access door in the test sample, can be represented by an equivalent magnetic dipole and an equivalent electric dipole. These

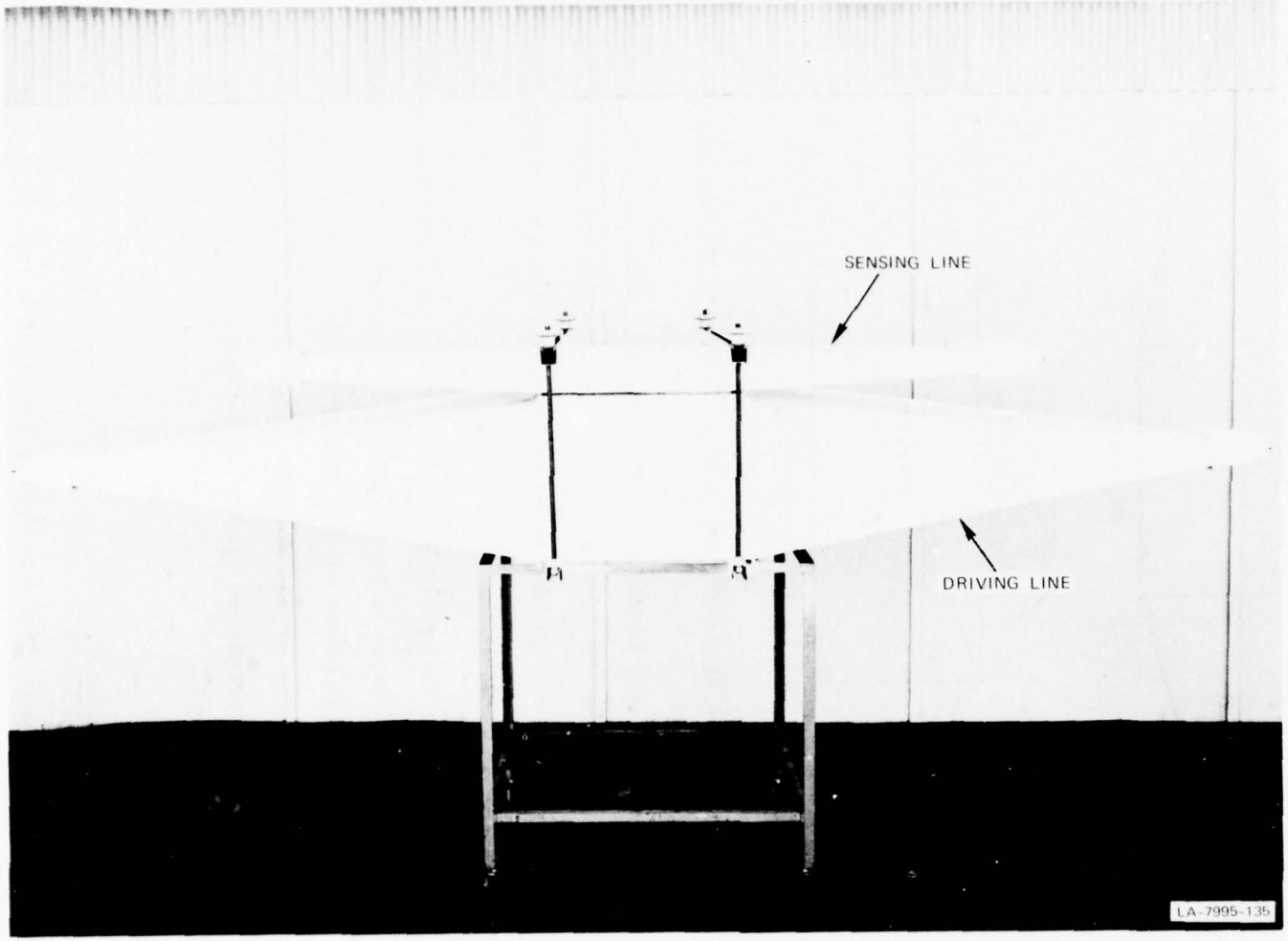

FIGURE A-2 PHOTOGRAPH OF RECTANGULAR COAXIAL SKIN TESTER

equivalent dipoles, whose strength is proportional to the ambient magnetic and electric fields in the driving line, produce electromagnetic fields in the sensing line. These fields induce transmission-line waves propagating in both directions in the sensing line; however, because the electric dipole couples symmetrically to the sensing line and the magnetic dipole couples asymmetrically to the line, the voltage (or current) observed with a matched termination is different at the two ends of the line.

The coupled transmission lines are illustrated schematically in Figure 3. At the receiving end of the sensing line the voltage across a matched termination is

$$V_r = j\omega K \frac{V_o}{2Z_o} [M - P] \qquad (1)$$

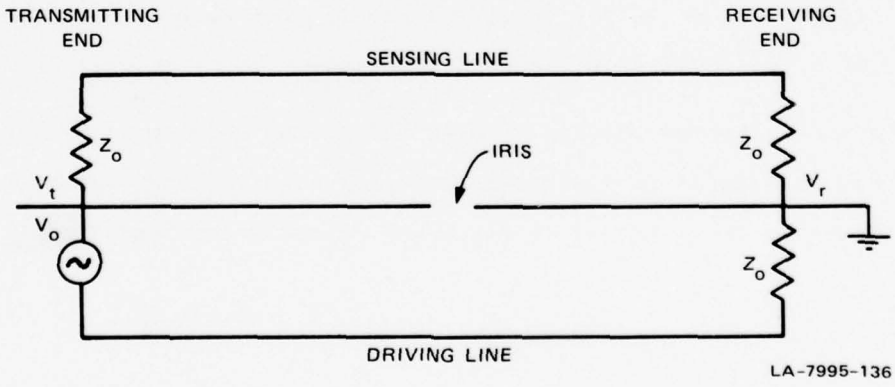

FIGURE A-3 IRIS-COUPLED TRANSMISSION LINES

where V_o is the voltage in the driving line, Z_o is the characteristic impedance of the sensing line and driving line, and K is a coupling constant associated with the geometry of the sensing line. The terms M and P are the magnetic and electric polarizabilities of the coupling

iris; these are the equivalent dipole moments normalized to the magnetic flux $\mu_o H$ and the electric flux $\epsilon_o E$, respectively, incident on the iris in the driving line. At the transmitting end of the sensing line the voltage across a matched termination is

$$V_t = j\omega K \frac{V_o}{2Z_o} [M + P] \quad . \tag{2}$$

For concentric coaxial transmission lines of circular cross section,

$$K = \frac{\mu_o}{4\pi^2 a^2} \tag{3}$$

where a is the radius of the common conductor. For transmission lines of rectangular cross section the value of K is not readily calculable, but for the skin tester it can be determined from measurements with an iris of known polarizability. From tests with a single 4-inch-diameter circular hole in a test panel, the value of K was found to be 1.43×10^{-6} H/m^3, while for the 1/2-inch-diameter holes 1 inch apart, $K_d = 2.97 \times 10^{-7}$ H/m^3 (for magnetic coupling).

By measuring the voltage at each end of the sensing line with the other end terminated in a matched load, the electric and magnetic polarizabilities of the joint or access panel can be determined from

$$P = \frac{Z_o}{j\omega V_o K} [V_t - V_r] \tag{4}$$

$$M = \frac{Z_o}{j\omega V_o K} [V_t + V_r] \tag{5}$$

where

V_o = Voltage applied to the driving line

Z_o = 50 ohms = Characteristic impedance of the driving and sensing lines

K = Geometric coupling factor for the facility

V_r = Voltage across a 50-ohm load at the receiving end of the sensing line

V_t = Voltage across a 50-ohm load at the transmitting end of the sensing line.

The transmission line voltage V_o is obtained from a plate (small dipole) antenna located in the driving line opposite the test panel. The voltage V_p developed across a 50-ohm load at the terminals of the plate antenna is calibrated in terms of the driving-line voltage V_o and the electric field E_o between the center conductor and the wide side wall. A small loop antenna is similarly located in the driving line. The voltage V_ℓ developed across a 50-ohm load at the terminals of the loop antenna is calibrated in terms of the driving-line voltage V_o and in terms of the magnetic field H_o at the side wall.

C. Specifications

Specifications for the skin-tester components are as follows:

(1) Driving line (rectangular coax)

- Impedance: 50 ohms
- Power rating: 500 watts
- Dimensions:
  - Test section: 15 × 36 inches (20-inch wide center plate)
  - Overall length: 146 inches
- Test-panel size: 20 × 20 inches.

(2) Sensing line (rectangular coax)

- Impedance: 50 ohms
- Dimensions:
  - Test section: 4-1/2 × 20 inches (6-1/2-inch-wide center plate)
  - Overall length: 102 inches.

(3) Geometric coupling coefficient

- Single iris: $K_1 = 1.43 \times 10^{-6}$ H/m
- Distributed iris: $K_d = 2.97 \times 10^{-7}$ H/m (magnetic)
  $K_d = 2.71 \times 10^{-7}$ H/m (electric).

(4) Sensing Antennas:

- Plate antenna: 4 inches in diameter, 1 cm high

$$V_o = 5.3 \times 10^9 \frac{V_p}{f}$$
$$E_o = 2.9 \times 10^9 \frac{V_p}{f}$$

with 50-ohm load

C = 12 pF

High-frequency 3-dB point: 250 MHz.

- Loop antenna: 4 inches long, 1 inch high

$$V_o = 3.5 \times 10^9 \frac{V_\ell}{f}$$
$$H_o = 4.9 \times 10^7 \frac{V_\ell}{f}$$

with 50-ohm load

L = 0.14 μH

High-frequency 3-dB point: 50 MHz.

(5) Connectors: All connectors are Type N; adapters for APC-7 connectors are provided.

Appendix B

SUBSURFACE HEMP FIELD CALCULATION

by

G. H. Price
Senior Physicist

May 1, 1975

Appendix B

SUBSURFACE HEMP FIELD CALCULATION

I INTRODUCTION

The electromagnetic pulse (EMP) interaction threat is nominally specified in terms of the free-space field. However, this specification is not always directly useful. Particularly in the case of buried structures, the field characteristics in the vicinity of the system are much modified from their free-space form. The objective here is to calculate the subsurface electric and magnetic fields corresponding to a nominal high-altitude EMP threat for a representative geometry.

II FREE-SPACE FIELD

The free-space electric field is taken to be

$$E(t) = E_o(1 - e^{-t/t_1})e^{-t/t_2} \tag{1}$$

with

$t_1 = 3.5\ \mu s$

$t_2 = 275\ \mu s$

$E_o = 50$ kV/m.

The corresponding magnetic field is given by

$$H(t) = \frac{1}{Z_o} E(t) \tag{2}$$

where $Z_o = (\mu_o/\epsilon_o)^{\frac{1}{2}} = 377\ \Omega$ is the impedance of free space with μ_o the permeability and ϵ_o the permittivity of free space, respectively. These free-space fields are illustrated in Figure 1.

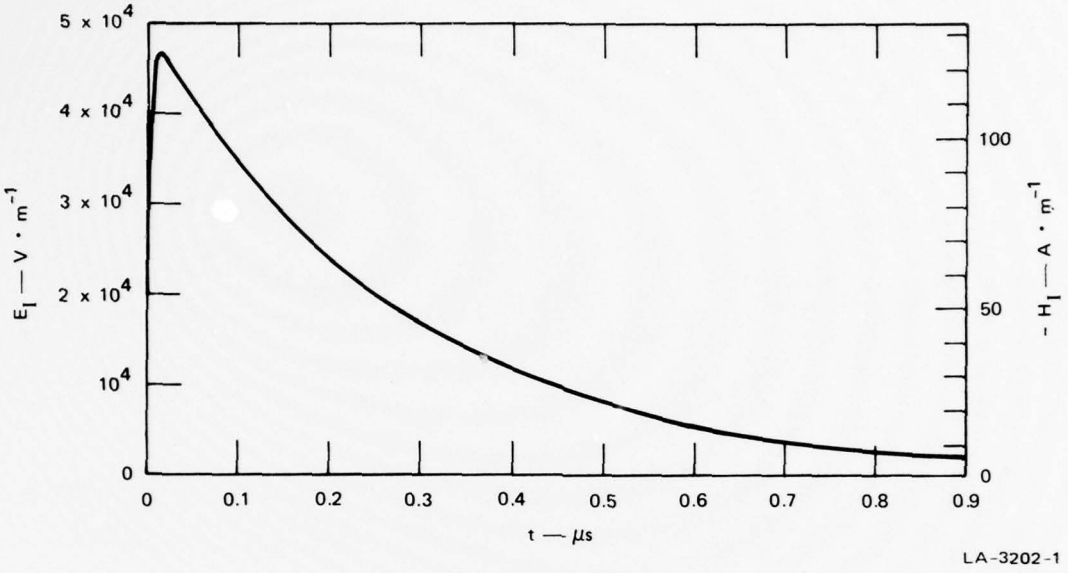

FIGURE B-1 INCIDENT PULSE

III FIELDS IN THE EARTH

A. Formulation

The penetration of the incident pulse into the earth is modeled as a straight forward, planar reflection/transmission problem, as shown in Figure 2. The earth's surface is taken to be the plane $x = 0$, with $x > 0$ free space and $x < 0$ within the earth. The earth is assumed to be a homogeneous, lossy dielectric characterized by a conductivity σ, a permittivity ϵ, and a permeability equal to that of free space--$\mu = \mu_o$.

With this model, the field expressions for a time-harmonic incident wave are well known. For a wave of angular frequency ω, incident at an angle θ_o from the vertical (x axis) with its electric field parallel to the surface (i.e., transverse electric) the sub-surface electric field $\vec{E}_t(\omega)$ is given by[1]

$$\vec{E}_t(\omega) = \vec{E}_1(\omega) \exp(ik_1\vec{n}_1 \cdot \vec{r} - i\omega t) \qquad (3)$$

[1] J. A. Stratton, Electromagnetic Fields, (McGraw-Hill Book Company, New York, 1941).

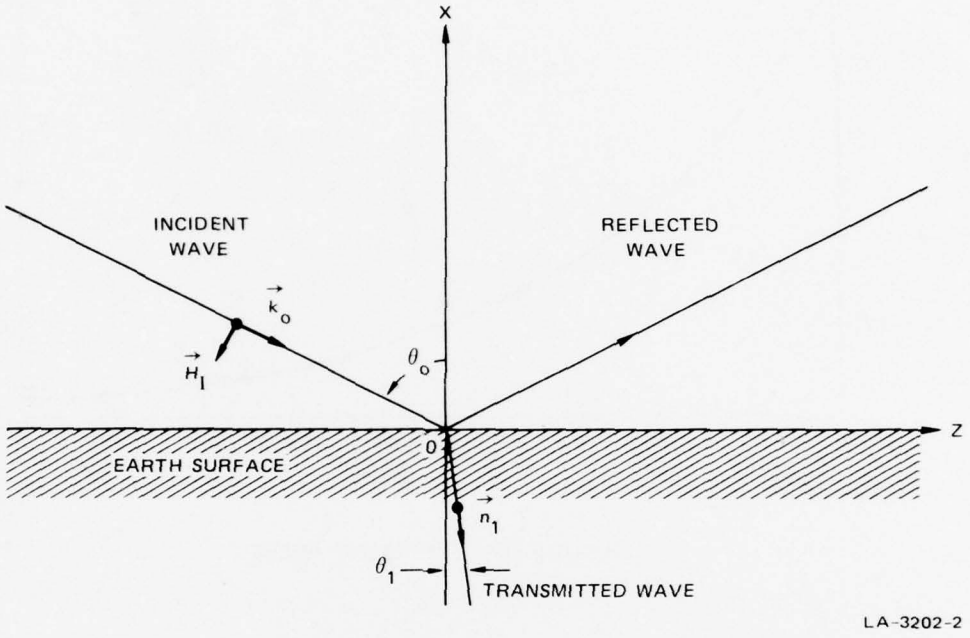

FIGURE B-2 GEOMETRY

with

$$\vec{E}_1(\omega) = \frac{2\cos\theta_o}{\cos\theta_o + \left[\left(\frac{k_1}{k_2}\right)^2 - \sin^2\theta_o\right]^{1/2}} \vec{E}_i(\omega) \ . \tag{4}$$

The wave numbers k_1 and k_2 are given by

$$k_1 = \left(\frac{\epsilon}{\epsilon_o} - \frac{\sigma}{i\omega\epsilon_o}\right) k_o \tag{5a}$$

$$k_2 = k_o = \frac{\omega}{c} \ , \tag{5b}$$

where c is the speed of light in free space. The subscripts 1 and 2 denote the regions within the earth and in free space, respectively.

The vector $\vec{n}_1$ is a unit vector in the direction of the wave normal within the earth, at an angle θ_1 relative to the negative x axis; this direction is determined by Snell's law

$$k_1 \sin \theta_1 = k_o \sin \theta_o \ . \tag{6}$$

Since k_1 is complex, so is θ_1, and $\vec{n}_1 \cdot \vec{r}$ has both real and imaginary components, describing the phase and amplitude variation, respectively, of the wave within the earth. If the electric field in the incident pulse is taken to be parallel to the y axis, $\vec{n}_1$ lies in the x - z plane and

$$\vec{n}_1 \cdot \vec{r} = - x \cos\theta_1 + z \sin\theta_1 \ . \tag{7}$$

The spectral components $\vec{E}_i(\omega)$ are given by the Fourier transform of the incident pulse. With our choice of the incident electric field parallel to the y axis,

$$\vec{E}_i(\omega) = \hat{i}_y \int_o^\infty dt \ e^{i\omega t} \ E(t) \ , \tag{8}$$

where $\hat{i}_y$ is a unit vector parallel to this axis. The integral is readily evaluated analytically for the E(t) given by Eq. (1), to give

$$E_i(\omega) = E_o \left(\frac{t_2}{1 - i\omega t_2} - \frac{t_c}{1 - i\omega t_c} \right) \tag{9}$$

where

$$t_c = \frac{t_1 t_2}{t_1 + t_2} \ . \tag{10}$$

The magnetic field within the earth is given in terms of $\vec{E}_t$ and $\vec{n}_1$ by

$$\vec{H}_t(\omega) = \frac{k_1}{\mu_o \omega} \vec{n}_1 \times \vec{E}_t \ . \tag{11}$$

Explicitly, Eq. (11) can be worked through to obtain

$$H_{t_x} = -\frac{E_t}{Z_o}\sin\theta_o \tag{12a}$$

$$H_{t_z} = -\frac{E_t}{Z_o}\left[\left(\frac{k_1}{k_2}\right)^2 - \sin^2\theta_o\right]^{1/2} \tag{12b}$$

where E_t is given by Eq. (3).

B. Results

The above equations have been used to calculate the sub-surface electric and magnetic fields in typical soil, $\sigma = 3 \times 10^{-3}$ mho $\cdot$ m^{-1} and $\epsilon = 10\ \epsilon_o$, for a pulse obliquely incident upon the earth's surface at an angle $\theta_o = 70°$. The magnitude of the spectral components $E_t(\omega)$ and $H_t(\omega)$ are shown in Figure 3 at depths of 0, 10, and 20 m, along with those of the incident electric field calculated from Eq. (9). The magnetic field, H_t, is elliptically polarized; that is, the magnetic field vector $\vec{H}_t(\omega)$ rotates in the x - z plane with its tip tracing out an ellipse. The magnitude of the major semi-axis of this ellipse (which lies nearly parallel to the z axis for our example) has been plotted in Figure 3 to represent H_t. The scales of the E and H axes have been deliberately chosen to produce the coalescence of the E and H spectra seen at the high frequencies.

The time-domain fields corresponding to these spectra are shown in Figure 4. Since the major semi-axis of the H_t ellipse does not lie in a fixed direction as a function of frequency, the major component of $\vec{H}_t$, $H_H = -H_{t_z}$, has been Fourier transformed to give the magnetic fields shown in Figure 4. The onset of the field is increasingly delayed with increasing depth beneath the surface as a result of the time required for the field to propagate to that depth. The time origin has been taken to correspond to the onset of the incident pulse at the point on the surface vertically above the field-observation point.

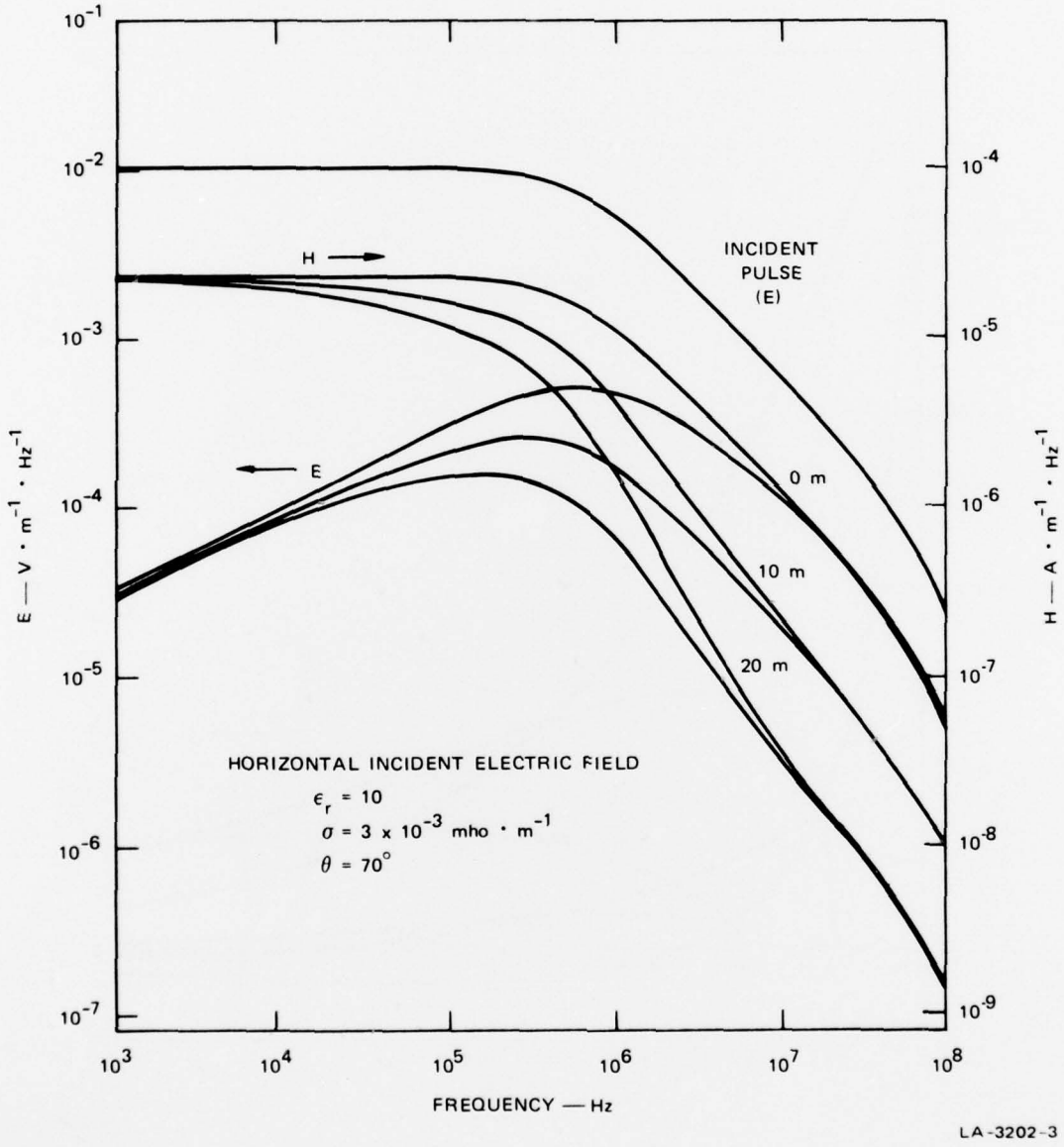

FIGURE B-3 SPECTRA OF ELECTRIC AND MAGNETIC FIELDS AT VARIOUS DEPTHS

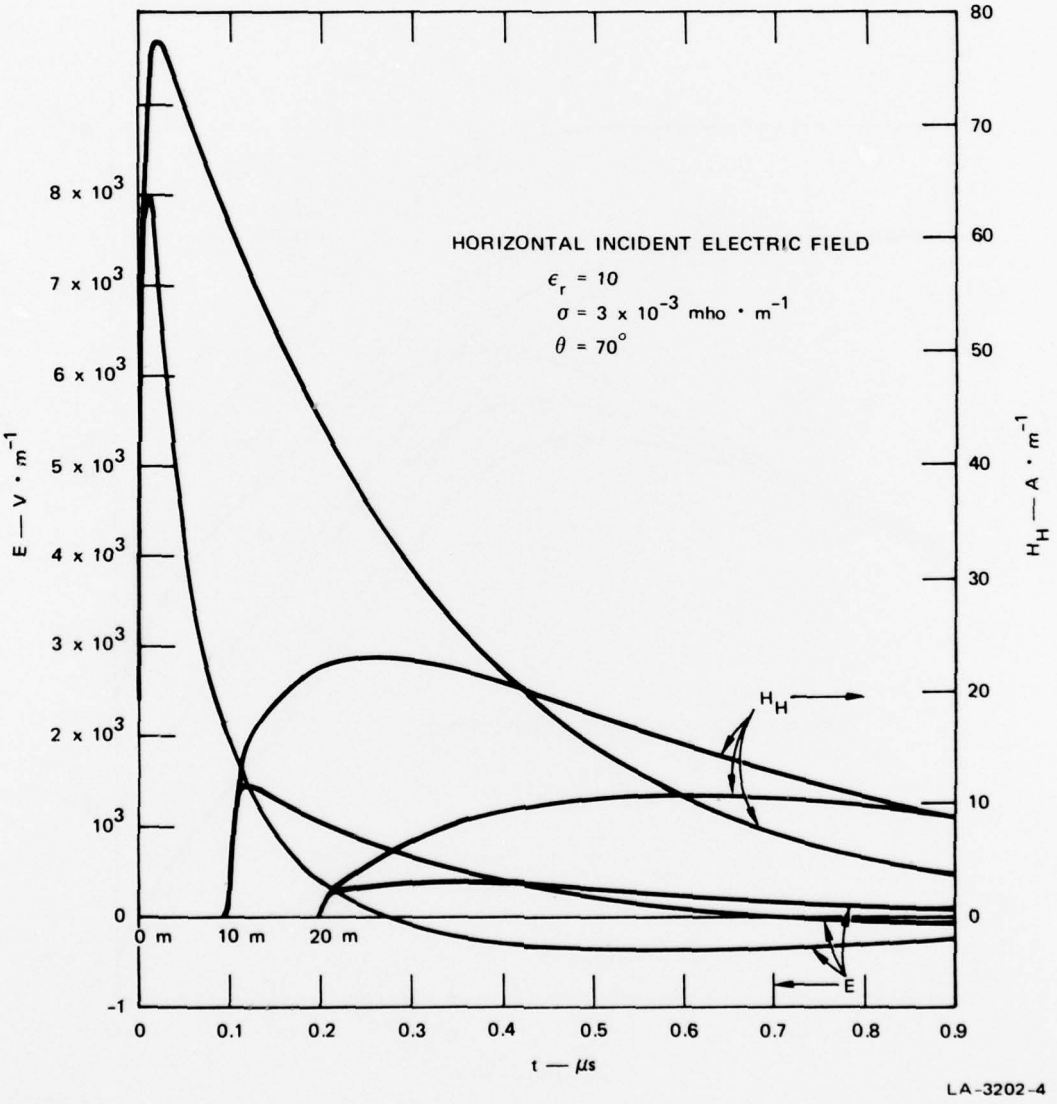

FIGURE B-4 ELECTRIC AND MAGNETIC FIELDS AT VARIOUS DEPTHS

The greater loss beneath the surface of the low-frequency spectral components in E relative to those in H that is evident in their spectra, Figure 3, is also apparent when their waveforms are compared for a given depth. The H_H waveforms consistently show a later and less sharp peak than do those for E. Also evident in both E and H waveforms is the progressive loss of the higher-frequency spectral components with increasing depth. This loss is manifest both in the increasing delay of the field peak and in the reduced slope of the initial field buildup with increasing depth. This last behavior is shown in greater detail in Figures 5, 6 and 7 in which E and H_H are plotted individually.

The reduction in the initial rate of change (slope) of the fields with increasing depth is of particular interest for the magnetic field since its coupling effectiveness tends to be proportional to dH/dt. In order to provide a more quantitative measure of the reduction of dH/dt with increasing depth, the spectra of H_H were modified (by multiplication by $-i\omega$) and inverse transformed to give $dH_H(t)/dt$. The peak values of dH_H/dt scaled from these waveforms are given in Table 1 as fractions of the peak dH/dt in the incident pulse. As can be seen from the table, the reduction in dH/dt beneath the surface is indeed marked. It should also be noted that the reduction in dH/dt is appreciable even at the surface. Since the horizontal magnetic field must be continuous across the surface, this reduction is also relevent to unburied systems located on the surface.

Table B-1

PEAK RATE OF CHANGE OF MAGNETIC FIELD RELATIVE TO THAT IN INCIDENT PULSE

Depth (m)	$(dH_H/dt)_{peak}/(dH_I/dt)_{peak}$
0	0.174
10	0.029
20	0.005

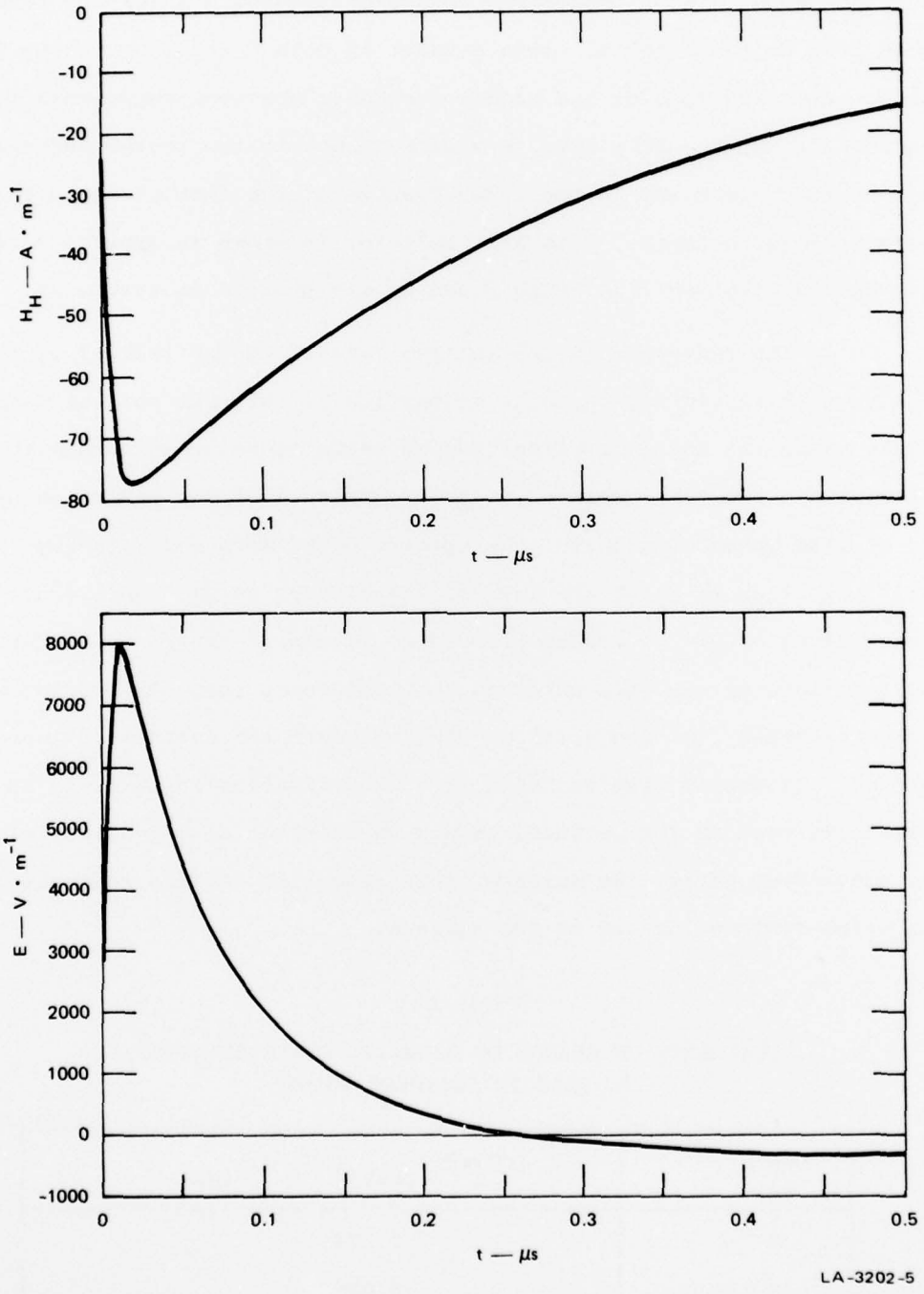

FIGURE B-5 HORIZONTAL MAGNETIC AND ELECTRIC FIELDS AT 0 m (surface)

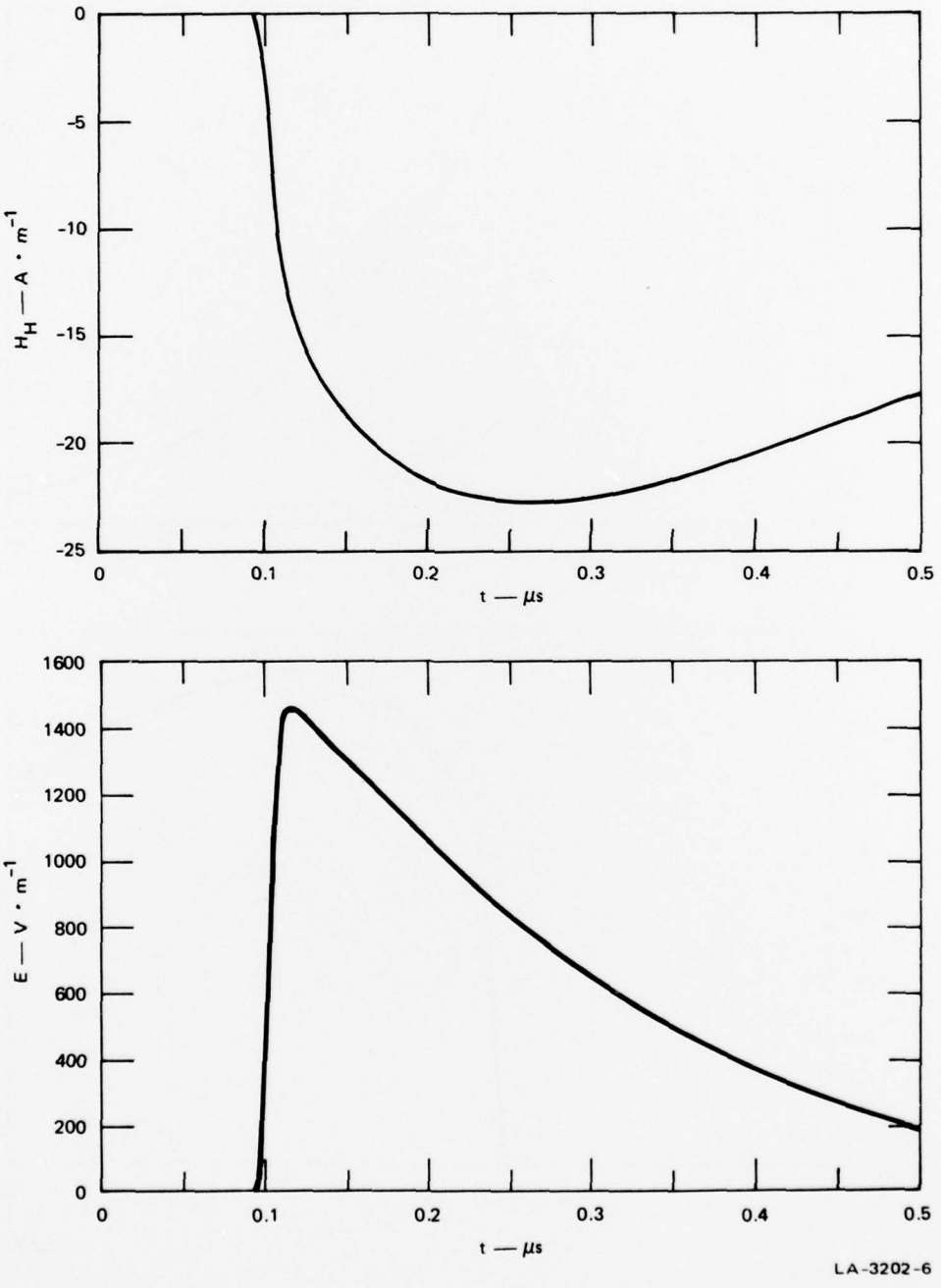

FIGURE B-6 HORIZONTAL MAGNETIC AND ELECTRIC FIELDS AT 10 m DEPTH

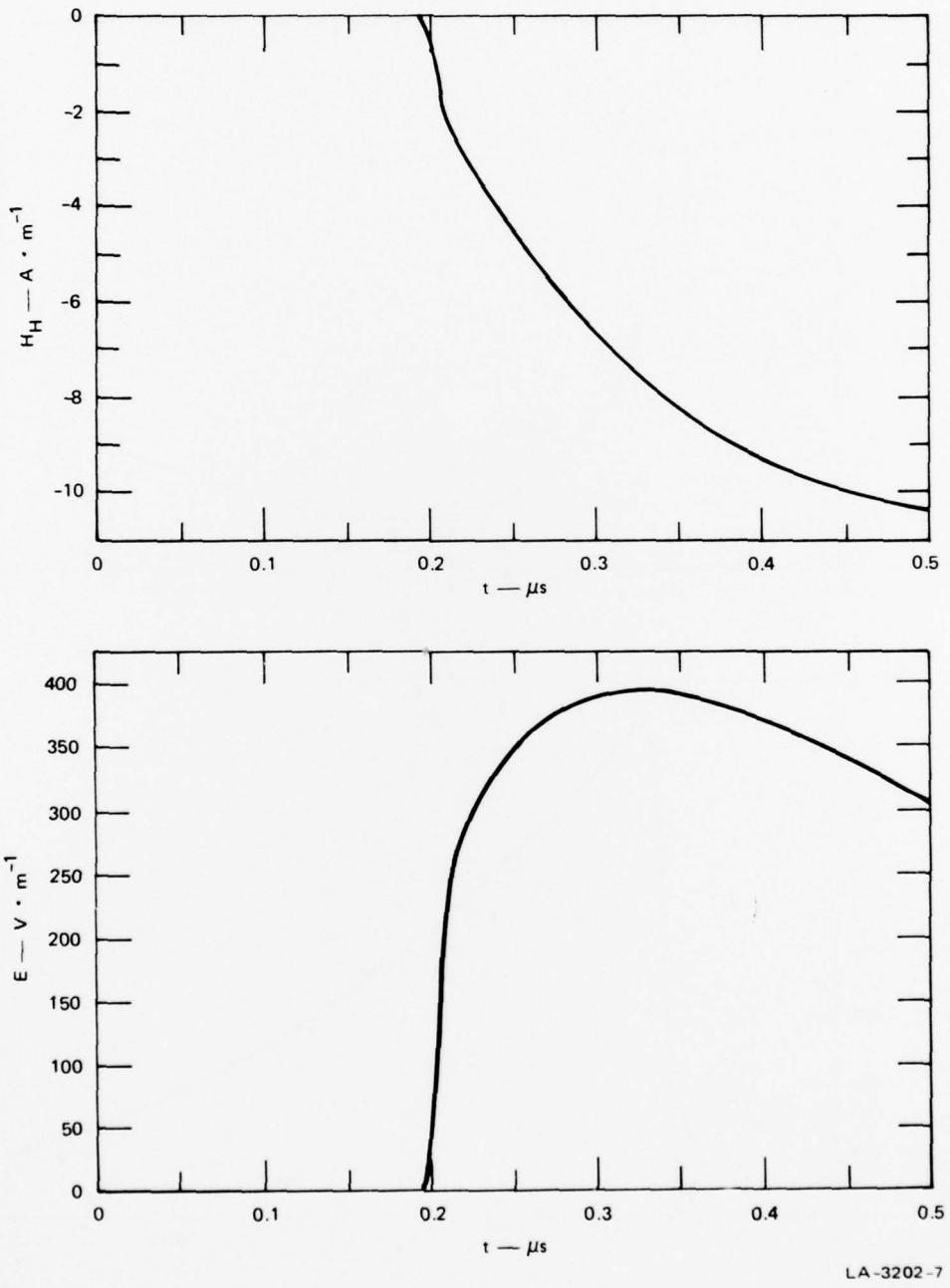

FIGURE B-7 HORIZONTAL MAGNETIC AND ELECTRIC FIELDS AT 20 m DEPTH

DISTRIBUTION LIST

DEPARTMENT OF DEFENSE

Assistant Secretary of Defense
Cmd., Cont., Comm. & Intell.
ATTN: I&W/IRA
ATTN: ODDDI (P&R)
ATTN: Dep. Dir. Telecomm. Systems

Assistant to the Secretary of Defense
Atomic Energy
ATTN: B. Adams

Director
Command Control Technical Center
ATTN: MD718

Commander in Chief, Pacific
ATTN: J-620

Director
Defense Advanced Rsch. Proj. Agency
ATTN: Technical Library
ATTN: AD/E&PS

Director
Armed Forces Radiobiology Research Institute
Defense Nuclear Agency
ATTN: RPC

Director
Defense Civil Preparedness Agency
Assistant Director for Research
ATTN: PO (SE)
ATTN: Admin. Officer
ATTN: TS, AED
ATTN: RE (EO)

Defense Communication Engineer Center
ATTN: Code R720, C. Stansberry
ATTN: Code R400
ATTN: Code R123, Tech. Library
ATTN: Code R720

Director
Defense Communications Agency
ATTN: Code 101B
ATTN: WWMCCS Sys. Engr.
ATTN: CCTC/C672
ATTN: Code 930, Monte I. Burgett, Jr.

Defense Communications Agency
WWMCCS System Engineering Org.
ATTN: Thomas Neighbors

Commander
Defense Communications Agency
Pacific Area
ATTN: Commander

Defense Documentation Center
Cameron Station
12 cy ATTN: TC

Director
Defense Intelligence Agency
ATTN: DT
ATTN: RDS-3A
ATTN: RDS-3A4, Pomponio Plaza

DEPARTMENT OF DEFENSE (Continued)

Director
Defense Nuclear Agency
ATTN: RAEV
ATTN: RAAE
ATTN: TISI, Archives
ATTN: DDST
ATTN: RATN
ATTN: STVL
2 cy ATTN: VLIS
3 cy ATTN: TITL, Tech. Library

Director of Planning & Evaluation
Office of the Secretary of Defense
ATTN: Dep. Dir. Gen. Pur. Prgms.

Commander
Field Command, DNA
ATTN: FCPR
ATTN: FCLM, CDR D. J. Griffiths
ATTN: FCLCM

Director
Joint Strat. Tgt. Planning Staff
ATTN: JLTW-2
ATTN: JPST
ATTN: STINFO Library

Chief
Livermore Division, Field Command, DNA
Lawrence Livermore Laboratory
ATTN: FCPRL

National Communications System
Office of the Manager
ATTN: NCS-TS
ATTN: NCS-TS, Charles Bodson

Director
National Security Agency
ATTN: Tech. Library
ATTN: TDL
ATTN: R-425

Director
Interservice Nuclear Weapons School
ATTN: Doc. Con.

Chief
National Security Agency
Central Sec. Serv. Pac. Area
ATTN: Central Sec. Serv. Pac. Area

OJCS/J-3
ATTN: J-3, WWMCCS & Telecommunications
ATTN: Cmd. & Control/Telecom. Sys.
ATTN: J-3

OJCS/J-5
ATTN: J-5, Nuc/Bio/Chem Branch
ATTN: J-5, SAGA

Under Secy. of Defense for Rsch. & Engrg.
ATTN: S&SS (OS)
ATTN: G. Barse

DEPARTMENT OF DEFENSE (Continued)

Supreme Hqs. Allied Powers Europe
100 cy ATTN: U.S. Documents Officer for
SPO Project "85"

DEPARTMENT OF THE ARMY

Chief C-E Services Division
U.S. Army Communications Cmd.
ATTN: CEEO-7

Commander
BDM System Command
ATTN: BMDSC-AOLIB

Commander
Harry Diamond Laboratories
ATTN: DELHD-TI, Tech. Library
ATTN: DELHD-EM, John Bombardt
ATTN: DELHD-NP
ATTN: DELHD-RBA
ATTN: DELHD-EM, Chief, EME Lab.
ATTN: DELHD-TF, Robert B. Oswald, Jr.
ATTN: DELHD-EM-5
ATTN: DELHD-EM-4
ATTN: DELHD-RB
ATTN: DELHD-TD
ATTN: DELHD-EM, Robert McCoskey
ATTN: DELHD-RB, Joseph R. Miletta
2 cy ATTN: DELHD-EM-2
2 cy ATTN: DELHD-RCC
3 cy ATTN: DELHD-EM-1
4 cy ATTN: DELHD-EM
5 cy ATTN: DELHD-EM-3

Deputy Chief of Staff for Rsch. Dev. & Acq.
ATTN: DAMA-CSM-N

Hqs., Department of the Army
ATTN: DAMA-TCV-A

Project Manager
Army Tactical Data Systems
ATTN: DRCAM-TDS-BSI

Project Manager
Multi-Service Communications Systems
ATTN: DRCPM-MSCS

Chief
U.S. Army Communications Sys. Agency
ATTN: CCM-RD-T, CCM-AD-SV
ATTN: SCCM-AD-SV, Library

Commander
U.S. Army CINCPAC Support Group
ATTN: Communications-Electronics

Commander
U.S. Army Comm-Elec. Engrg. Instal. Agy.
ATTN: ACCC-CED-STS
ATTN: CCC-PRSO-S

Commander
U.S. Army Communications Cmd.
ATTN: ACC-FD-C/EMP
ATTN: CC-OPS-PD
ATTN: CC-OPS-OS

DEPARTMENT OF THE ARMY (Continued)

Commander
U.S. Army Computer Systems Command
ATTN: Tech. Library

Commander
U.S. Army Missile Command
ATTN: DRDMI-TRR, F. P. Gibson
ATTN: DRDMI-TBD
ATTN: DRDMI-EAA
ATTN: DRCPM-PF-EA, Wallace D. Wagner
ATTN: DRCPM-PE-EG, William P. Johnson

Commander
U.S. Army Nuclear & Chemical Agency
ATTN: Library

Commander
U.S. Army Tank Automotive Cmd.
ATTN: DRCPM-GCM-SW, Lyle A. Wolcott

Commander
U.S. Army Training and Doctrine Comd.
ATTN: ATORI-OP-SW

Commander
White Sands Missile Range
ATTN: TE-AN, Mr. Okuma
ATTN: D. E. Miller

Director
U.S. Army Materiel Sys. Analysis Acty.
ATTN: DRXSY-PO

DEPARTMENT OF THE NAVY

Chief of Naval Operations
ATTN: OP 98
ATTN: OP 94

Chief of Naval Research
ATTN: Tech. Library

Commander
Naval Electronic Systems Command
ATTN: Tech. Library
ATTN: PME 117-T
ATTN: PME 117-215

Commander
Naval Ocean Systems Center
ATTN: Tech. Library
ATTN: Research Library
ATTN: Code 812, S. W. Lichtman

Superintendent (Code 1424)
Naval Postgraduate School
ATTN: Code 2124, Tech. Rpts. Librarian
ATTN: Code 1424

Director
Naval Research Laboratory
ATTN: Code 2600, Tech. Library
ATTN: Code 2627, Doris Folen
ATTN: Code 6624

DEPARTMENT OF THE NAVY (Continued)

Commander
Naval Air Systems Command
ATTN: AIR 350F

Commander
Naval Sea Systems Command
ATTN: SEA-9931

Commander
Naval Ship Engineering Center
ATTN: Code 6174D2
ATTN: Code 6174D2, Edward Duffy

Commander
Naval Telecommunications Command
ATTN: Deputy Director Systems

Commanding Officer
Naval Ordnance Station
ATTN: Standardization Dept.

Officer-in-Charge
Civil Engineering Laboratory
ATTN: Tech. Library

Officer-in-Charge
Naval Surface Weapons Center
ATTN: Code WA51
ATTN: WA50
ATTN: Code 431, Edwin R. Rathburn
ATTN: Code WA51RH, Rm. 130-108
ATTN: Code WR43, L. Libello

Commander
Naval Weapons Center
ATTN: Code 533, Tech. Library

Director
Strategic Systems Project Office
ATTN: NSP-43, Tech. Library
ATTN: SP 2701, John W. Pitsenberger

Commander-in-Chief
U.S. Pacific Fleet
ATTN: N5

DEPARTMENT OF THE AIR FORCE

AF Communications Service
ATTN: XP

AF Security Service
ATTN: XRX

AF Weapons Laboratory, AFSC
ATTN: SUL
ATTN: ELC
ATTN: EL
ATTN: EL, Library
ATTN: NTO
ATTN: NT, Carl Baum
ATTN: ELXT
ATTN: CA
ATTN: ELA, J. D. Castillo
ATTN: ELP

Assistant Chief of Staff
Studies and Analysis
ATTN: AF/SA

DEPARTMENT OF THE AIR FORCE (Continued)

Assistant Chief of Staff
Communications & Computer Resources
ATTN: AF/KRC

Commander
Air University
ATTN: AUL/LSE-70-250

Commander
ASD
ATTN: ENFTV

Assistant Deputy Chief of Staff
Research and Development
ATTN: RDQ/SN

Headquarters
Electronic Systems Division, AFSC
ATTN: Tech. Library

Commander
Foreign Technology Division, AFSC
ATTN: NICD Library
ATTN: ETD, B. L. Ballard

Commander in Chief
Pacific Air Forces
ATTN: Communications-Electronics

Commander
Rome Air Development Center, AFSC
ATTN: EMTLD Doc. Library
ATTN: TSLD

SAMSO/DY
ATTN: DYS

SAMSO/SK
ATTN: SKF

Command in Chief
Strategic Air Command
ATTN: XPFS
ATTN: NRI-STINFO Library
ATTN: DEL
ATTN: Garnet E. Matzke
ATTN: XPFS, Maj Brian G. Stephan

Commander
Ogden Air Logistics Center
ATTN: OO-ALC/MMETH, P. W. Berthel
ATTN: MMEDO, Leo Kidman
ATTN: Maj Ronald Blackburn

SAMSO/IN
ATTN: IND, I. J. Judy

SAMSO/MN
ATTN: MNNH, Capt R. I. Lawrence
ATTN: MNNH, Maj M. Baran

SAMSO/YA
ATTN: YAPC

DEPARTMENT OF ENERGY

Department of Energy
Albuquerque Operations Office
ATTN: Doc. Con. for Tech. Library

DEPARTMENT OF ENERGY (Continued)

University of California
Lawrence Livermore Laboratory
ATTN: Librarian
ATTN: Terry R. Donich, L-96
ATTN: Hans Kruger, L-96

Los Alamos Scientific Laboratory
ATTN: Doc. Con. for Clarence Benton

Sandia Laboratories
ATTN: Doc. Con. for Org. 9353, R. L. Parker

OTHER GOVERNMENT AGENCIES

Central Intelligence Agency
ATTN: RD/SI, Rm. 5G48, Hq. Bldg. for OSI/NED/NWB

Administrator
Defense Electric Power Admin.
Department of the Interior
ATTN: L. O'Neill

Department of Transportation
Federal Aviation Administration
ATTN: Sec. Div., ASE-300

DEPARTMENT OF DEFENSE CONTRACTORS

Aerospace Corporation
ATTN: Irving M. Garfunkel
ATTN: Library
ATTN: Julian Reinheimer
ATTN: C. B. Pearlston

Agbabian Associates
ATTN: Library

American Telephone & Telegraph Co.
Administrative Office
ATTN: M. J. Gray for W. L. Edwards

Avco Research & Systems Group
ATTN: W. Lepsevich

Battelle Memorial Institute
ATTN: Robert H. Blazek
ATTN: Eugene R. Leach

The BDM Corporation
ATTN: L. Jacobs
ATTN: Tech. Library

The BDM Corporation
ATTN: Tech. Library

The Boeing Company
ATTN: David Kemle
ATTN: B. C. Hanrahan
ATTN: D. E. Isbell
ATTN: Kent Tech. Library
2 cy ATTN: E. Nowak, MS 47/14

Booz-Allen and Hamilton, Inc.
ATTN: Tech. Library
ATTN: Raymond J. Chrisner

DEPARTMENT OF DEFENSE CONTRACTORS (Continued)

Brown Engineering Company, Inc.
Cummings Research Park
ATTN: Fred Leonard

Burroughs Corporation
Federal and Special Systems Group
ATTN: Angelo J. Mauriello

Calspan Corporation
ATTN: Tech. Library

Charles Stark Draper Laboratory, Inc.
ATTN: TIC, MS 74
ATTN: Kenneth Fertig

Cincinnati Electronics Corporation
ATTN: Lois Hammond

Computer Sciences Corporation
ATTN: H. Blank
ATTN: Ramona Briggs

Computer Sciences Corporation
ATTN: Alvin T. Schiff

Control Data Corporation
ATTN: Jack Meehan

Cutler-Hammer, Inc.
AIL Division
ATTN: Edward Karpen

Dikewood Industrires, Inc.
ATTN: L. Wayne Davis
ATTN: Tech. Library

E-Systems, Inc.
ECI Division
ATTN: Raymond D. Frank

E-Systems, Inc.
Greenville Division
ATTN: Joleta Moore

Effects Technology, Inc.
ATTN: S. Clow

EG&G, Inc.
ATTN: C. Giles

ESL, Inc.
ATTN: James Marshall

Ford Aerospace & Communications Corporation
ATTN: J. T. Mattingley, MS X22
ATTN: Library

Ford Aerospace & Communications Operations
ATTN: E. R. Poncelet, Jr.
ATTN: Ken C. Attinger

General Dynamics Corporation
ATTN: Rsch. Library

General Dynamics Corporation
Inter-Division Research Library
ATTN: Research Library

DEPARTMENT OF DEFENSE CONTRACTORS (Continued)

General Electric Company
Ordnance Systems
ATTN: Joseph J. Reidl

General Electric Company
TEMPO-Center for Advanced Studies
ATTN: DASIAC
ATTN: Royden R. Rutherford
ATTN: William McNamera

General Electric Company-TEMPO
c/o Defense Nuclear Agency
ATTN: DASIAC for Ed Arno'd
ATTN: DASIAC for William Alfonte

Georgia Institute of Technology
Georgia Tech. Research Institute
ATTN: R. Curry

Grumman Aerospace Corporation
ATTN: L-01 35

GTE Sylvania, Inc.
Electronics Systems Grp.-Eastern Div.
ATTN: Charles A. Thornhill, Librarian

GTE Sylvania, Inc.
ATTN: J. A. Waldron
ATTN: Comm. Sys. Div., Marshall Cross
ATTN: David P. Flood
ATTN: Comm. Sys. Div., Emil P. Motchok
ATTN: H&V Group, Mario A. Nurefora
ATTN: Charles H. Ramsbottom

Harris Corporation
Harris Semiconductor Division
ATTN: V. Pres. & Mgr. Prgms. Div.

Honeywell, Inc.
Avionics Division
ATTN: Ronald R. Johnson, A1622
ATTN: S&RC Library

Honeywell, Inc.
Avionics Division
ATTN: W. E. Stewart
ATTN: MS 725-5, Stacey H. Graff

Hughes Aircraft Company
ATTN: John B. Singletary, MS 6-D133
ATTN: CTOC 6/E110

IIT Research Institute
ATTN: Jack E. Bridges
ATTN: Irving N. Mindel

Institute for Defense Analyses
ATTN: Tech. Info. Ofc.
ATTN: IDA Librarian, Ruth S. Smith

Intl. Tel. & Telegraph Corporation
ATTN: Tech. Library

IRT Corporation
ATTN: C. B. Williams
ATTN: Dennis Swift

[illegible]
ATTN: W. A. Radasky

DEPARTMENT OF DEFENSE CONTRACTORS (Continued)

JAYCOR
ATTN: Ralph H. Stahl
ATTN: Eric P. Wenaas

JAYCOR
ATTN: Tech. Library

Kaman Sciences Corporation
ATTN: Walter E. Ware
ATTN: Frank H. Shelton
ATTN: W. Foster Rich
ATTN: Albert P. Bridges
ATTN: Jerry I. Lubell

Litton Systems, Inc.
ATTN: EMC Gp.
ATTN: M848-61

Litton Systems, Inc.
ATTN: J. Skaggs

Lockheed Missiles & Space Co., Inc.
ATTN: H. E. Thayn
ATTN: George F. Heath, Dept. 81-14
ATTN: L. Rossi, Dept. 81-64
ATTN: Samuel I. Taimuty, Dept. 85-85

Lockheed Missiles & Space Co., Inc.
ATTN: Tech. Info. Ctr., D/Coll.

M.I.T. Lincoln Laboratory
ATTN: Leona Loughlin, Librarian, A-082

Martin Marietta Corporation
ATTN: Mona C. Griffith, Lib., MP-30

Maxwell Laboratories, Inc.
ATTN: A. W. Travelpiece

McDonnell Douglas Corporation
ATTN: Tom Ender

McDonnell Douglas Corporation
ATTN: Tech. Library Services
ATTN: Stanley Schneider

Mission Research Corporation
ATTN: William C. Hart
ATTN: EMP Group

Mission Research Corporation
EM System Applications Division
ATTN: L. N. McCormick
ATTN: David E. Merewether

Mission Research Corporation-San Diego
ATTN: V. A. J. Van Lint

The Mitre Corporation
ATTN: Mr. Schulstad
ATTN: Theodore Jarvis
ATTN: M. E. Fitzgerald

Northrop Corporation
Northrop Research and Technology Ctr.
ATTN: Library

Physics International Company
ATTN: Doc. Con.

DEPARTMENT OF DEFENSE CONTRACTORS (Continued)

Northrop Corporation
ATTN: Lew Smith
ATTN: Tech. Library
ATTN: Vincent R. DeMartino

Pulsar Associates, Inc.
ATTN: Security

R&D Associates
ATTN: William R. Graham, Jr.
ATTN: Leonard Schlessinger
ATTN: B. Gage
ATTN: Doc. Con.
ATTN: S. Clay Rogers
ATTN: Richard R. Schaefer
ATTN: Charles Mo

The Rand Corporation
ATTN: LIB-D

Ray Proof Corporation
ATTN: E. S. Kesner

Raytheon Company
ATTN: Gajanan H. Joshi, Radar Sys. Lab.

Raytheon Company
ATTN: Harold L. Flescher

RCA Corporation
Government Systems Division
ATTN: George J. Brucker

RCA Corporation
Camden Complex
ATTN: Olive Whitehead
ATTN: Ed Van Keuren

Rockwell International Corporation
ATTN: V. J. Michel
ATTN: J. L. Monroe, Dept. 243-027, Div. 031
ATTN: Dept. 243-068, 031-CA31

Rockwell International Corporation
ATTN: B. E. White

Rockwell International Corporation
ATTN: B-1, Div. TIC (BAOB)

DEPARTMENT OF DEFENSE CONTRACTORS (Continued)

Science Applications, Inc.
ATTN: Frederick M. Tesche

Science Applications, Inc.
ATTN: R. Parkinson

Science Applications, Inc.
ATTN: William L. Chadsey

The Singer Company
ATTN: Security Manager for Tech. Info. Ctr.

Sperry Flight Systems Division
ATTN: D. Andrew Schow

Sperry Rand Corporation
ATTN: Tech. Library

Spire Corporation
ATTN: Roger G. Little

SRI International
ATTN: Arthur Lee Whitson
ATTN: George Carpenter
ATTN: Ed F. Vance

SRI International
ATTN: Mr. Hullings

Texas Instruments, Inc.
ATTN: Donald J. Manus, MS 72
ATTN: Tech. Library

Texas Tech University
ATTN: Travis L. Simpson

TRW Defense & Space Sys. Group
ATTN: O. E. Adams, RI-1144
ATTN: L. R. Magnolia

United Technologies Corporation
Norden Division
ATTN: Tech. Library

Westinghouse Electric Corporation
Advanced Energy Systems Div.
ATTN: Tech. Library